arXiv:1211.4011v1 [hep-ph] 16 Nov 2012

IMPLEMENTING HILLTOP F-TERM HYBRID INFLATION IN SUPERGRAVITY

R. ARMILLIS[(1)] **AND C. PALLIS**[(2)]

[(1)]*Institut de Théorie des Phénomenès Physiques,*
École Polytechnique Fédérale de Lausanne,
BSP 730 Cubotron, CH-1015 Lausanne, SWITZERLAND
roberta.armillis@epfl.ch

[(2)]*Department of Physics, University of Cyprus,*
P.O. Box 20537, CY-1678 Nicosia, CYPRUS
cpallis@ucy.ac.cy

ABSTRACT

F-term hybrid inflation (FHI) of the hilltop type can generate a scalar spectral index, $n_{\rm s}$, in agreement with the fitting of the seven-year Wilkinson microwave anisotropy probe data by the standard power-law cosmological model with cold dark matter and a cosmological constant, ΛCDM. We investigate the realization of this type of FHI by using quasi-canonical Kähler potentials with or without the inclusion of extra hidden-sector fields. In the first case, acceptable results can be obtained by constraining the coefficients of the quadratic and/or quartic supergravity correction to the inflationary potential and therefore a mild tuning of the relevant term of the Kähler potential is unavoidable. Possible reduction of $n_{\rm s}$ without generating maxima and minima of the potential on the inflationary path is also possible in a limited region of the available parameter space. The tuning of the terms of the Kähler potential can be avoided with the adoption of a simple class of string-inspired Kähler potentials for the hidden-sector fields which ensures a resolution to the η problem of FHI and allows acceptable values for the spectral index, constraining the coefficient of the quartic supergravity correction to the inflationary potential. Performing a four-point test of the analyzed models, we single out the most promising of these.

KEYWORDS: Cosmology, Inflation
PACS CODES: 98.80.Cq, 11.30.Pb

1 PROLOGUE

Inflation [1] has been incredibly successful in providing solutions to the problems of the *Standard Big Bang cosmology* (SBB). It can set the initial conditions, which give rise to the high degree of flatness and homogeneity that we observe in the universe today. From particle physics motivated models, it not only yields a mechanism for accelerated expansion but also explains, through quantum fluctuations, the origin of the temperature anisotropies in the *Cosmic Microwave Background* (CMB) and the seeds for the observed Large Scale Structure – for reviews see e.g. Refs. [2, 3].

We focus on a set of well-motivated, popular and quite natural models of *supersymmetric* (SUSY) *F-term hybrid inflation* (FHI) [4]. Namely, we consider the standard [5] FHI and some of its specific versions: the shifted [6] and smooth [7] FHI. They are realized [5] at (or close to) the SUSY *Grand Unified Theory* (GUT) scale $M_{\rm GUT} \simeq 2.86 \cdot 10^{16}$ GeV and can be easily linked to several extensions [3] of the *Minimal Supersymmetric Standard Model* (MSSM) which have a rich structure. Namely, the μ-problem of MSSM is solved via a direct coupling of the inflaton to Higgs superfields [8] or via a Peccei-Quinn symmetry [9], baryon number conservation is an automatic consequence [8] of an R symmetry and the baryon asymmetry of the universe is generated via leptogenesis which takes place [10] through the out-of-equilibrium decays of the inflaton's decay products.

Although quite successful, these models have at least two shortcomings:

(i) The problem of the enhanced (scalar) spectral index, $n_{\rm s}$. It is well-known that under the assumption that the problems of SBB are resolved exclusively by FHI, these models predict $n_{\rm s}$ just marginally consistent with the fitting of the seven-year results [11] from the *Wilkinson Microwave Anisotropy Probe Satellite* (WMAP7) data with the standard power-law cosmological model with *cold dark matter and a cosmological constant* (ΛCDM).

(ii) The so-called η problem. This problem is tied [2, 4, 12] on the expectation that *supergravity* (SUGRA) corrections generate a mass squared for the inflaton of the order of the Hubble parameter during FHI and so, the η criterion is generically violated, ruining thereby FHI. Inclusion of SUGRA corrections with canonical Kähler potential prevents [4, 13, 14] the generation of such a mass term due to a mutual cancellation. However, despite its simplicity, the canonical Kähler potential can be regarded [4] as fine tuning to some extent and, in all cases, increases $n_{\rm s}$ even more.

In this topical review we reconsider one set of possible resolutions (for other proposals, see Ref. [15, 16, 17, 18]) of the tension between FHI and the data. This is relied on the utilization of three types of quasi-canonical [19] Kähler potential with or without the inclusion of extra fields, h_m. The term "extra fields" refers to hidden-sector [20] fields or fields which do not participate [21] in the inflationary superpotential but may only affect the Kähler potential. The consideration of extra fields assists us in solving the η problem of FHI as well. In particular, we review the following embeddings of FHI in SUGRA:

(i) FHI in *next-to-minimal SUGRA* (nmSUGRA) – see Sec. 5. A convenient choice of the next-to-minimal term [22, 23, 24] of the Kähler potential leads to a negative mass (quadratic) term for the inflaton and therefore $n_{\rm s}$ can be diminished sizeably.

(ii) FHI in *next-to-next-to-minimal SUGRA* (nnmSUGRA) – see Sec. 6. A convenient choice of the next-to-minimal and the next-to-next-to-minimal term generates [25, 26] a positive mass (quadratic) term for the inflaton and a sizeable negative quartic term which yield acceptable $n_{\rm s}$ enhancing somehow the running of $n_{\rm s}$, $\alpha_{\rm s}$.

(iii) FHI with extra fields, h_m, obeying a string-inspired Kähler potential (hSUGRA) – see Sec. 7. In the presence of h_m's, we can establish [27] a type of hilltop FHI which avoids the tuning – required in the cases (i) and (ii) above – of the quadratic SUGRA correction and is largely dominated by the quartic SUGRA correction. Namely, the coefficients of the Kähler potential are constrained to natural values (of order unity) so as the mass term of the inflaton field is identically zero.

In all the cases above and in the largest part of the parameter space the inflationary potential acquires a local maximum and minimum. Then, FHI of the hilltop type [28] can occur as the inflaton rolls from this maximum down to smaller values. However, the value of the inflaton field at the maximum is to be sufficiently close to the value that this field acquires when the pivot scale crosses outside the inflationary horizon. Therefore, $n_{\rm s}$ can become consistent with data, but only at the cost of an extra indispensable mild tuning [22] of the initial conditions. Another possible complication is that the system may get trapped near the minimum of the inflationary potential, thereby jeopardizing the attainment of FHI. On the other hand, we can show [23] that acceptable $n_{\rm s}$'s can be obtained even maintaining the monotonicity of the inflationary potential, i.e. without this minimum-maximum problem in the case of nmSUGRA.

In this presentation we reexamine the above ideas for the reduction of $n_{\rm s}$ within FHI, updating our results in Ref. [24, 27] and incorporating recent related developments in Ref. [25]. In particular, the text is organized as follows: In Sec. 2, we review the basic FHI models and in Sec. 4 we recall the results holding for FHI in *minimal SUGRA* (mSUGRA). In the following we demonstrate how we can obtain hilltop FHI using various types of Kähler potentials – see Secs 5, 6 and 7. Our conclusions are summarized in Sec. 8. Throughout the text, charge conjugation is denoted by a star and brackets are, also, used by applying disjunctive correspondence.

2 FHI WITHIN SUGRA

We outline the salient features of the basic types of FHI. Namely we present the relevant superpotentials in Sec 2.1 and the SUSY potentials in Sec. 2.2. We then (in Sec. 2.3) describe the embedding of these models in SUGRA and extract the relevant inflationary potential in Sec. 2.4.

2.1 THE RELEVANT SUPERPOTENTIAL

The F-term hybrid inflation can be realized adopting one of the superpotentials below:

$$W = \widehat{W} + W_{\text{FHI}} \text{ with } W_{\text{FHI}} = \begin{cases} \widehat{\kappa} S \left(\bar{\Phi}\Phi - M^2 \right) & \text{for standard FHI,} \\ \widehat{\kappa} S \left(\bar{\Phi}\Phi - M^2 \right) - S \frac{(\bar{\Phi}\Phi)^2}{M_{\text{S}}^2} & \text{for shifted FHI,} \\ S \left(\frac{(\bar{\Phi}\Phi)^2}{M_{\text{S}}^2} - \widehat{\mu}_{\text{S}}^2 \right) & \text{for smooth FHI,} \end{cases} \tag{1}$$

where we allow for the presence of a part, $\widehat{W}$, which depends exclusively on the hidden sector superfields, h_m. Here (and hereafter) we use the hat to denote such quantities. To keep our analysis as general as possible, we do not adopt any particular form for $\widehat{W}$ – for some proposals see Ref. [29, 30]. Note that our construction remains intact even if we set $\widehat{W} = 0$ as it was supposed in Ref. [21]. This is due to the fact that $\widehat{W}$ is expected to be much smaller than the inflationary energy density – see Sec. 2.3. For $\widehat{W} \neq 0$, though, we need to assume that h_m's are stabilized before the onset of FHI by some mechanism not consistently taken into account here. As a consequence, we neglect the dependence of $\widehat{W}$, $\widehat{\kappa}$ and $\widehat{\mu}_{\text{S}}$ on h_m and so, these quantities are treated as constants. We further assume that the D-terms due to h_m's vanish – contrary to the strategy adopted in Ref. [21].

The remaining symbols in the *right hand side* (r.h.s) of Eq. (1) are identified as follows:

- S is a left handed superfield, singlet under a GUT gauge group G;

- $\bar{\Phi}$, Φ is a pair of left handed superfields belonging to non-trivial conjugate representations of G, and reducing its rank by their *vacuum expectation values* (v.e.vs);

- $\widehat{M}_{\text{S}} \sim 5 \times 10^{17}$ GeV is an effective cutoff scale comparable with the string scale;

- $\widehat{\kappa}$ and $\widehat{M}$, $\widehat{\mu}_{\text{S}}$ ($\sim M_{\text{GUT}}$) are parameters which can be made positive by field redefinitions.

The superpotential in Eq. (1) for standard FHI is the most general renormalizable superpotential consistent with a continuous R-symmetry [5] under which

$$S \to e^{ir} S, \ \bar{\Phi}\Phi \to \bar{\Phi}\Phi, \ W \to e^{ir} W. \tag{2}$$

After including in this superpotential the leading non-renormalizable term, one obtains the superpotential of shifted [6] FHI in Eq. (1). Finally, the superpotential of smooth [7] FHI can be obtained if we impose an extra Z_2 symmetry under which the combination $\bar{\Phi}\Phi$ has unit charge.

2.2 THE SUSY POTENTIAL

The SUSY potential, V_{SUSY}, extracted (see e.g. ref. [2]) from W_{FHI} in Eq. (1) includes F and D-term contributions. Namely,

$$V_{\text{SUSY}} = V_{\text{F}} + V_{\text{D}}, \tag{3}$$

where

(i) The F-term contribution can be written as:

$$V_{\mathrm{F}} = \begin{cases} \kappa^2 M^4 \left((\Phi^2 - 1)^2 + 2S^2\Phi^2\right) & \text{for standard FHI,} \\ \kappa^2 M^4 \left((\Phi^2 - 1 - \xi\Phi^4)^2 + 2S^2\Phi^2(1 - 2\xi\Phi^2)^2\right) & \text{for shifted FHI,} \\ \mu_{\mathrm{S}}^4 \left((1 - \Phi^4)^2 + 8S^2\Phi^6\right) & \text{for smooth FHI,} \end{cases} \quad (4)$$

where the scalar components of the superfields are denoted by the same symbols as the corresponding superfields and $\xi = M^2/\kappa M_{\mathrm{S}}^2$ with $4 < 1/\xi < 7.2$ [6]. In order to recover the properly normalized energy density during FHI, we absorb in the constants of Eq. (4) some normalization pre-factors emerging from the SUGRA potential V_{SUGRA} – see below – so that their definition is

$$\kappa = e^{\widehat{K}/2m_{\mathrm{P}}^2} \widehat{Z}^{-1/2} \widehat{\kappa}, \quad \mu_{\mathrm{S}} = e^{\widehat{K}/4m_{\mathrm{P}}^2} \widehat{Z}^{-1/4} \widehat{\mu}_{\mathrm{S}} \ \text{and} \ M_{\mathrm{S}} = e^{-\widehat{K}/4m_{\mathrm{P}}^2} \widehat{Z}^{1/4} \widehat{M}_{\mathrm{S}} \quad (5)$$

where $\widehat{K}$ and $\widehat{Z}$ are the h_m-dependent parts of the Kähler potential, K, considered in Sec. 2.3. The last relation is introduced so as $\kappa M_{\mathrm{S}}^2 = \widehat{\kappa}\widehat{M}_{\mathrm{S}}^2$ and $\mu_{\mathrm{S}} M_{\mathrm{S}} = \widehat{\mu}_{\mathrm{S}}\widehat{M}_{\mathrm{S}}$. Also, we use [6, 7] the following dimensionless quantities

$$\begin{cases} \Phi = |\Phi|/M \ \text{and} \ \mathsf{S} = \widehat{Z}^{1/2}|S|/M & \text{for standard or shifted FHI,} \\ \Phi = |\Phi|/\sqrt{\mu_{\mathrm{S}} M_{\mathrm{S}}} \ \text{and} \ \mathsf{S} = \widehat{Z}^{1/2}|S|/\sqrt{\mu_{\mathrm{S}} M_{\mathrm{S}}} & \text{for smooth FHI.} \end{cases} \quad (6)$$

In Fig. 1-(a), Fig. 1-(b) and 2 we present the three dimensional plot of V_{F} versus $\pm\Phi$ and S for standard, shifted and smooth FHI, respectively.

(ii) The D-term contribution V_{D} vanishes for $|\bar{\Phi}| = |\Phi|$ since V_{D} has the form:

$$V_{\mathrm{D}} = \frac{1}{2}g^2 \sum_a D_a D_a \ \text{with} \ D_a = \phi_M (T_a)_N^M K^{\bar{N}} \simeq |\Phi|^2 - |\bar{\Phi}|^2, \quad (7)$$

where g is the (unified) gauge coupling constant, T_a are the generators of G and the notation used is explained below Eq. (11) – recall that Φ and $\bar{\Phi}$ belong to the conjugate representation of G.

From the form of V_{SUSY} in Eq. (4), we can understand that W in Eq. (1) plays a twofold crucial role:

(i) It leads to the spontaneous breaking of G. Indeed, the vanishing of V_{F} gives the v.e.vs of the fields in the SUSY vacuum. Namely,

$$\langle S \rangle = 0 \ \text{and} \ |\langle\bar{\Phi}\rangle| = |\langle\Phi\rangle| = v_G = \begin{cases} M & \text{for standard FHI,} \\ \frac{M\sqrt{1 - \sqrt{1 - 4\xi}}}{\sqrt{2\xi}} & \text{for shifted FHI,} \\ \sqrt{\mu_{\mathrm{S}} M_{\mathrm{S}}} & \text{for smooth FHI} \end{cases} \quad (8)$$

(in the case where $\bar{\Phi}$, Φ are not *Standard Model* (SM) singlets, $\langle\bar{\Phi}\rangle$, $\langle\Phi\rangle$ stand for the v.e.vs of their SM singlet directions). The non-zero value of the v.e.v v_G signalizes the spontaneous breaking of G.
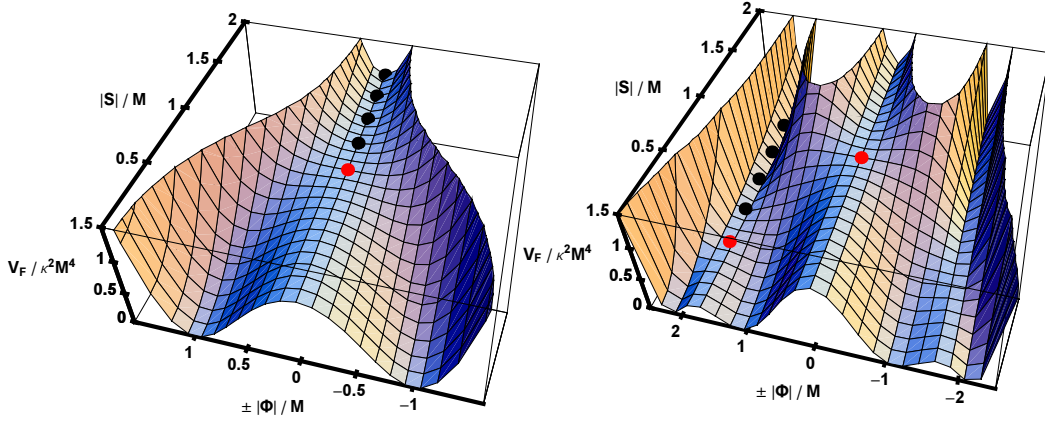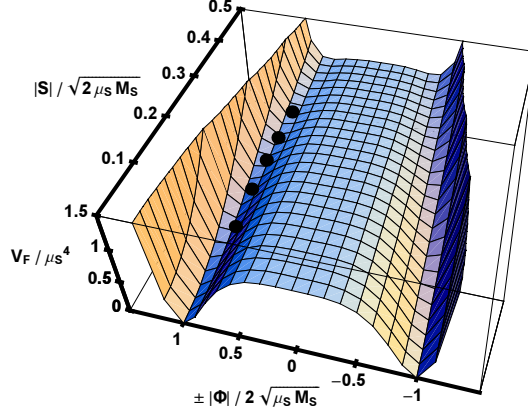
FIGURE 1: *The three dimensional plot of the (dimensionless) F-term potential $V_{\rm F}/\kappa^2 M^4$ versus $\mathsf{S} = |S|/M$ and $\pm\Phi = \pm|\Phi|/M$ for standard [shifted with $\xi = 1/6$] FHI (left [right]). The inflationary trajectories are also depicted by black points whereas the critical points (of the shifted and standard trajectories) are depicted by red/light points.*

(ii)   It gives rise to FHI. This is due to the fact that, for large enough values of $|S|$, there exist valleys of local minima of the classical potential with constant (or almost constant in the case of smooth FHI) values of $V_{\rm F}$. In particular, we can observe that $V_{\rm F}$ takes the following constant value

$$V_{\rm HI0} = \begin{cases} \kappa^2 M^4 \\ \kappa^2 M_\xi^4 \\ \mu_{\rm S}^4 \end{cases} \text{along the direction(s):} \quad \Phi = \begin{cases} 0 & \text{for standard FHI,} \\ 0 \text{ or } 1/\sqrt{2\xi} & \text{for shifted FHI,} \\ 0 \text{ or } 1/2\sqrt{3}\mathsf{S} & \text{for smooth FHI,} \end{cases} \quad (9)$$

with $M_\xi = M\sqrt{1/4\xi - 1}$. From Figs. 1 and 2 we deduce that the flat direction $\Phi = 0$ corresponds to a minimum of $V_{\rm F}$, for $|S| \gg M$, in the cases of standard and shifted FHI and to a maximum of $V_{\rm F}$ in the case of smooth FHI. The inflationary trajectories are depicted by bold points, whereas the critical points by red/light points. Note that critical points exist only in the case of standard – for $\mathsf{S} = 1$ – and shifted – for $\mathsf{S} = (1/4\xi - 1)/2$ – FHI but not for smooth FHI. In the case of Fig. 1-(b), the implementation of shifted FHI is ensured by restricting $1/\xi$ in the range $(4 - 7.2)$ [6]. Under this assumption, the shifted track lies lower that the trivial one and so, it is energetically more favorable to drive FHI.

   Since FHI can be attained along a minimum of $V_{\rm F}$, we infer that, during standard FHI, the GUT gauge group G is necessarily restored. As a consequence, topological defects such as strings [31, 22], monopoles, or domain walls may be produced [7] via the Kibble mechanism [32] during the spontaneous breaking of G at the end of FHI. This can be avoided in the other two cases, since the form of $V_{\rm F}$ allows for non-trivial inflationary valleys along which G is spontaneously broken due to non-zero values that $\bar{\Phi}$ and Φ acquire during FHI. Therefore, no topological defects are produced in these cases.

FIGURE 2: *The three dimensional plot of the (dimensionless) F-term potential V_F/μ_S^4 for smooth FHI versus $\mathsf{S} = |S|/\sqrt{\mu_S M_S}$ and $\pm \Phi = \pm |\Phi|/\sqrt{\mu_S M_S}$. The inflationary trajectory is also depicted by black points.*

2.3 SUGRA CORRECTIONS

The consequences that SUGRA has on the models of FHI can be investigated by restricting ourselves to the inflationary trajectory $\Phi = \bar{\Phi} \simeq 0$ (possible corrections due to the non-vanishing Φ and $\bar{\Phi}$ in the cases of shifted and smooth FHI are expected to be negligible). Therefore, W in Eq. (1) takes the form

$$W = \widehat{W} + I, \text{ where } I = -\widehat{V}_{\mathrm{HI0}}^{1/2} S \text{ with } \widehat{V}_{\mathrm{HI0}} = e^{-\widehat{K}/m_{\mathrm{P}}^2} \widehat{Z} V_{\mathrm{HI0}}. \tag{10}$$

The SUGRA scalar potential (without the D-terms) is given (see, e.g., Ref. [2]) by

$$V_{\mathrm{SUGRA}} = e^{\frac{K}{m_{\mathrm{P}}^2}} \left(K^{M\bar{N}} F_M F_{\bar{N}}^* - 3\frac{|W|^2}{m_{\mathrm{P}}^2} \right) \text{ where } F_N = W_N + K_N \frac{W}{m_{\mathrm{P}}^2} \tag{11}$$

are the SUGRA-generalized F-terms, the subscript M [$\bar{M}$] denotes derivation *with respect to* (w.r.t) the complex scalar field ϕ_M [ϕ_M^*] which corresponds to the chiral superfield ϕ_M with $\phi_M = h_m, S, \Phi, \bar{\Phi}$ and the matrix $K^{M\bar{N}}$ is the inverse of the Kähler metric $K_{M\bar{N}}$. In this paper we consider a quite generic form of Kähler potentials, which do not deviate much from the canonical one and respect the R symmetry of Eq. (2). Namely we take

$$\begin{aligned} K &= \widehat{K} + \widehat{Z}|S|^2 + \frac{1}{4}k_{4S}\widehat{Z}^2\frac{|S|^4}{m_{\mathrm{P}}^2} + \frac{1}{6}k_{6S}\widehat{Z}^3\frac{|S|^6}{m_{\mathrm{P}}^4} + \frac{1}{8}k_{8S}\widehat{Z}^4\frac{|S|^8}{m_{\mathrm{P}}^6} \\ &\quad + \frac{1}{10}k_{10S}\widehat{Z}^5\frac{|S|^{10}}{m_{\mathrm{P}}^8} + \frac{1}{12}k_{12S}\widehat{Z}^6\frac{|S|^{12}}{m_{\mathrm{P}}^{10}} + |\Phi|^2 + |\bar{\Phi}|^2 + \cdots, \end{aligned} \tag{12}$$

where $k_{4S}, k_{6S}, k_{8S}, k_{10S}$ and k_{12S} are positive or negative constants of order unity and the ellipsis represents higher order terms involving the waterfall fields (Φ and $\bar{\Phi}$) and S. We can neglect these terms since they are irrelevant along the inflationary path.

Substituting Eq. (12) into Eq. (11) and expanding $V_{\rm SUGRA}$ in powers of $|S|$, we end up with an expansion of the form:

$$V_{\rm SUGRA} \simeq V_{\rm HI0}\left(1 - 2c_{1K}e^{-\frac{\widehat{K}}{2m_{\rm P}^2}}\frac{|\widehat{W}|\widehat{Z}^{1/2}}{\sqrt{V_{\rm HI0}}}|S|\cos\theta + \sum_{\nu=1}^{5}(-1)^{\nu}c_{2\nu K}\widehat{Z}^{\nu}\left(\frac{|S|}{m_{\rm P}}\right)^{2\nu}\right)$$
(13)

where the phase θ reads $\theta = \arg\widehat{W} + \arg S + \arg\widehat{V}_{\rm HI0}^{1/2}$. In the r.h.s of the expression above, we neglect terms proportional to $|\widehat{W}|^2$ which are certainly subdominant compared with those which are proportional to $V_{\rm HI}$. From the terms proportional to $|\widehat{W}|V_{\rm HI0}^{1/2}$ we present the second term of the r.h.s of Eq. (13) which expresses the most important contribution [14, 29] to the inflationary potential from the soft SUSY breaking terms. For natural values of $\widehat{W}$ and $e^{\widehat{K}/2m_{\rm P}^2}$ this term starts [14] playing an important role in the case of standard FHI in mSUGRA – see Sec. 4.2 – for $\kappa \lesssim 5 \cdot 10^{-4}$ whereas it has [14] no significant effect in the cases of shifted and smooth FHI.

Taking in Eq. (12) $\widehat{K} = 0$ and $\widehat{Z} = 1$ (as in Secs. 4 – 6) the coefficients $c_{\nu K} = c_{\nu K}^{(0)}$ are found to be

$$c_{1K}^{(0)} = -2,$$
(14a)

$$c_{2K}^{(0)} = k_{4S},$$
(14b)

$$c_{4K}^{(0)} = \frac{1}{2} - \frac{7k_{4S}}{4} + k_{4S}^2 - \frac{3k_{6S}}{2},$$
(14c)

$$c_{6K}^{(0)} = -\frac{2}{3} + \frac{3k_{4S}}{2} - \frac{7k_{4S}^2}{4} + k_{4S}^3 + \frac{10k_{6S}}{3} - 3k_{4S}k_{6S} + 2k_{8S},$$
(14d)

$$c_{8K}^{(0)} = \frac{3}{8} - \frac{5k_{10S}}{2} - \frac{13k_{4S}}{24} + \frac{41k_{4S}^2}{32} - \frac{7k_{4S}^3}{4} + k_{4S}^4 - \frac{13k_{6S}}{4}$$
$$+ \frac{143k_{4S}k_{6S}}{24} - \frac{9k_{4S}^2k_{6S}}{2} + \frac{9k_{6S}^2}{4} - \frac{39k_{8S}}{8} + 4k_{4S}k_{8S},$$
(14e)

$$c_{10K}^{(0)} = -\frac{2}{15} + \frac{32k_{10S}}{5} + 3k_{12S} + \frac{k_{4S}}{24} - 5k_{10S}k_{4S} - \frac{13k_{4S}^2}{24} + \frac{41k_{4S}^3}{32}$$
$$- \frac{7k_{4S}^4}{4} + k_{4S}^5 + \frac{5k_{6S}}{3} - \frac{29k_{4S}k_{6S}}{6} + \frac{103k_{4S}^2k_{6S}}{12} - 6k_{4S}^3k_{6S} - 5k_{6S}^2$$
$$+ \frac{27k_{4S}k_{6S}^2}{4} + 5k_{8S} - \frac{67k_{4S}k_{8S}}{8} + 6k_{4S}^2k_{8S} - 6k_{6S}k_{8S}.$$
(14f)

We observe that terms of order ν in the expansion of Eq. (12) give rise to contributions of order equal or greater than $(\nu - 2)$ in the expansion of Eq. (13).

2.4 THE INFLATIONARY POTENTIAL

The general form of the potential which can drive the various versions of FHI reads

$$V_{\rm HI} \simeq V_{\rm HI0}\left(1 + c_{\rm HI} - {\rm a}_S\frac{\sigma}{\sqrt{2V_{\rm HI0}}} + \sum_{\nu=1}^{5}(-1)^{\nu}c_{2\nu K}\left(\frac{\sigma}{\sqrt{2}m_{\rm P}}\right)^{2\nu}\right),$$
(15)

where $\sigma = \sqrt{2}\widehat{Z}^{1/2}|S|$ is the canonically (up to the order $|S|^2$) normalized inflaton field and we take $\theta = \pi$ which minimizes V_{SUGRA} for given σ. To facilitate our numerical analysis, we introduce the real tadpole parameter a_S defined in terms of the V_{SUGRA} parameter, by the relation

$$\text{a}_S = 2c_{1K}e^{-\widehat{K}/2m_{\text{P}}^2}|\widehat{W}|. \tag{16}$$

In Eq. (15), besides the contributions originating from V_{SUGRA} in Eq. (13), we include the term $c_{\text{HI}}V_{\text{HI0}}$ which represents a correction to V_{HI} resulting from the SUSY breaking on the inflationary valley, in the cases of standard [5] and shifted [6] FHI, or from the structure of the classical potential in the case of smooth [7] FHI. Indeed, $V_{\text{HI0}} > 0$ breaks SUSY and gives rise to logarithmic radiative corrections to the potential originating from a mass splitting in the $\Phi - \bar{\Phi}$ supermultiplets. On the other hand, in the case of smooth [7] FHI, the inflationary valleys are not classically flat and, thus, the radiative corrections are expected to be subdominant. The term c_{HI} can be written as follows:

$$c_{\text{HI}} = \begin{cases} \kappa^2\text{N}\left[2\ln\left(\kappa^2 x M^2/Q^2\right) + f_{\text{rc}}(x)\right]/32\pi^2 & \text{for standard FHI,} \\ \kappa^2\left[2\ln\left(\kappa^2 x_\xi M_\xi^2/Q^2\right) + f_{\text{rc}}(x_\xi)\right]/16\pi^2 & \text{for shifted FHI,} \\ -2\mu_{\text{s}}^2 M_{\text{S}}^2/27\sigma^4 & \text{for smooth FHI,} \end{cases} \tag{17}$$

with $x = \sigma^2/2M^2$, $x_\xi = \sigma^2/M_\xi^2$ and

$$f_{\text{rc}}(x) = (x+1)^2\ln(1+1/x) + (x-1)^2\ln(1-1/x) \Rightarrow f_{\text{rc}}(x) \simeq 3 \text{ for } x \gg 1. \tag{18}$$

Also N is the dimensionality of the representations to which $\bar{\Phi}$ and Φ belong and Q is a renormalization scale. For the values of κ encountered in our work renormalization group effects [33] remain negligible.

In our applications in Secs. 4.2, 5.3, 6.3 and 7.3 we take $\text{N} = 2$. This choice corresponds to the left-right symmetric GUT gauge group $SU(3)_c \times SU(2)_L \times SU(2)_R \times U(1)_{B-L}$ with $\bar{\Phi}$ and Φ belonging to $SU(2)_R$ doublets with $B - L = -1$ and 1 respectively. No cosmic strings are produced during the GUT phase transition and, consequently, no extra restrictions on the parameters (as e.g. in Refs. [31]) have to be imposed. As regards the case of shifted [6] FHI we identify G with the Pati-Salam gauge group $SU(4)_c \times SU(2)_L \times SU(2)_R$. Needless to say that the case of smooth FHI is independent on the adopted GUT since the inclination of the inflationary path is generated at the classical level and the addition of any radiative correction is expected to be subdominant. Negligible is also the third term in the r.h.s of Eq. (15) for $\text{a}_S \sim 1$ TeV, besides the case of standard FHI in mSUGRA – see Sec. 4 – where it may be important for $\kappa \leq 5 \cdot 10^{-4}$. For simplicity, we neglect it, in the analysis of the remaining cases – see Secs. 5, 6 and 7.

3 CONSTRAINING FHI

The parameters of FHI models can be restricted imposing a number of observational constraints described in Secs. 3.1 and 3.2. Additional theoretical considerations presented in Sec. 3.3 can impose further limitations.

3.1 INFLATIONARY OBSERVABLES

Applying standard formulae – see e.g. Refs. [2, 3] – we can estimate the inflationary observables of FHI. Namely, we can find:

(i) The number of e-foldings $N_{\mathrm{HI}*}$ that the scale $k_* = 0.002/\mathrm{Mpc}$ suffers during FHI,

$$N_{\mathrm{HI}*} = \frac{1}{m_{\mathrm{P}}^2} \int_{\sigma_{\mathrm{f}}}^{\sigma_*} d\sigma \, \frac{V_{\mathrm{HI}}}{V_{\mathrm{HI}}'}, \tag{19}$$

where the prime denotes derivation w.r.t σ, σ_* is the value of σ when the scale k_* crosses outside the horizon of FHI, and σ_{f} is the value of σ at the end of FHI, which can be found, in the slow roll approximation, from the condition

$$\mathsf{max}\{\epsilon(\sigma_{\mathrm{f}}), |\eta(\sigma_{\mathrm{f}})|\} = 1, \ \ \text{where} \ \ \epsilon \simeq \frac{m_{\mathrm{P}}^2}{2} \left(\frac{V_{\mathrm{HI}}'}{V_{\mathrm{HI}}}\right)^2 \ \ \text{and} \ \ \eta \simeq m_{\mathrm{P}}^2 \frac{V_{\mathrm{HI}}''}{V_{\mathrm{HI}}}. \tag{20}$$

In the cases of standard [5] and shifted [6] FHI and in the parameter space where the terms in Eq. (11) do not play an important role, the end of inflation coincides with the onset of the GUT phase transition, i.e. the slow roll conditions are violated close to the critical point $\sigma_{\mathrm{c}} = \sqrt{2}M$ [$\sigma_{\mathrm{c}} = M_\xi$] for standard [shifted] FHI, where the waterfall regime commences. On the contrary, the end of smooth [7] FHI is not abrupt since the inflationary path is stable w.r.t $\Phi - \bar{\Phi}$ for all σ's and σ_{f} is found from Eq. (20). An accurate enough estimation of σ_{f}'s – suitable for our analytical expressions presented below – is

$$\sigma_{\mathrm{f}} \simeq \begin{cases} \sqrt{2}M & \text{for standard FHI,} \\ M_\xi & \text{for shifted FHI,} \\ \sqrt{2\sqrt[3]{5}/3}\sqrt[3]{\mu_{\mathrm{S}}M_{\mathrm{S}}m_{\mathrm{P}}} & \text{for smooth FHI.} \end{cases} \tag{21}$$

(ii) The power spectrum $\Delta_{\mathcal{R}}^2$ of the curvature perturbations generated by σ at the pivot scale k_*

$$\Delta_{\mathcal{R}} = \frac{1}{2\sqrt{3}\,\pi m_{\mathrm{P}}^3} \left.\frac{V_{\mathrm{HI}}^{3/2}}{|V_{\mathrm{HI}}'|}\right|_{\sigma=\sigma_*}. \tag{22}$$

(iii) The spectral index

$$n_{\mathrm{s}} = 1 - 6\epsilon_* + 2\eta_*, \tag{23a}$$

its running

$$\alpha_{\mathrm{s}} = \frac{2}{3}\left(4\eta_*^2 - (n_{\mathrm{s}} - 1)^2\right) - 2\xi_*, \tag{23b}$$

with $\xi \simeq m_{\mathrm{P}}^4 \, V_{\mathrm{HI}}' V_{\mathrm{HI}}'''/V_{\mathrm{HI}}^2$ and the scalar-to-tensor ratio

$$r = 16\epsilon_* \tag{23c}$$

where all the variables with the subscript $*$ are evaluated at $\sigma = \sigma_*$.

3.2 OBSERVATIONAL CONSTRAINTS

Under the assumption that the contribution in Eq. (22) is solely responsible for the observed curvature perturbation – i.e. there are no contributions to $\Delta_{\mathcal{R}}$ from curvatons [2] or topological defects [31] – and (ii) there is a conventional cosmological evolution after FHI – see point (i) below –, the parameters of the FHI models can be restricted imposing the following requirements:

(i) The number of e-foldings $N_{\mathrm{HI*}}$ computed by means of Eq. (19) has to be set equal to the number of e-foldings N_* elapsed between the horizon crossing of the observationally relevant mode k_* and the end of FHI. N_* can be found as follows [2]:

$$
\begin{aligned}
\frac{k_*}{H_0 R_0} = \frac{H_* R_*}{H_0 R_0} &= \frac{H_*}{H_0} \frac{R_*}{R_{\mathrm{Hf}}} \frac{R_{\mathrm{Hf}}}{R_{\mathrm{rh}}} \frac{R_{\mathrm{rh}}}{R_{\mathrm{eq}}} \frac{R_{\mathrm{eq}}}{R_0} \\
&= \sqrt{\frac{V_{\mathrm{HI0}}}{\rho_{c0}}} e^{-N_*} \left(\frac{V_{\mathrm{HI0}}}{\rho_{\mathrm{rh}}}\right)^{-1/3} \left(\frac{\rho_{\mathrm{rh}}}{\rho_{\mathrm{eq}}}\right)^{-1/4} \left(\frac{\rho_{\mathrm{eq}}}{\rho_{m0}}\right)^{-1/3} \\
\Rightarrow \quad N_* &\simeq \ln \frac{H_0 R_0}{k_*} + 24.72 + \frac{2}{3} \ln \frac{V_{\mathrm{HI0}}^{1/4}}{1~\mathrm{GeV}} + \frac{1}{3} \ln \frac{T_{\mathrm{rh}}}{1~\mathrm{GeV}}, \quad (24)
\end{aligned}
$$

where T_{rh} is the reheating temperature after the completion of the FHI. Moreover, R is the scale factor, $H = \dot{R}/R$ is the Hubble rate, ρ is the energy density and the subscripts 0, k, Hf, rh, eq and m denote respectively values at the present (except for the symbol V_{HI0}), at the horizon crossing ($k = R_k H_k$) of the mode k, at the end of FHI, at the end of the reheating period, at the radiation-matter equidensity point and in the matter dominated era. In our calculation we take into account that $R \propto \rho^{-1/3}$ for decaying-particle domination or matter dominated era and $R \propto \rho^{-1/4}$ for radiation dominated era. We use the following numerical values:

$$
\rho_{c0} = 8.099 \times 10^{-47} h_0^2 ~\mathrm{GeV}^4 ~\mathrm{with}~ h_0 = 0.71, \tag{25a}
$$

$$
\rho_{\mathrm{rh}} = \frac{\pi^2}{30} g_{\rho*} T_{\mathrm{rh}}^4 ~\mathrm{with}~ g_{\rho*} = 228.75, \tag{25b}
$$

$$
\rho_{\mathrm{eq}} = 2\Omega_{m0}(1 - z_{\mathrm{eq}})^3 \rho_{c0} ~\mathrm{with}~ \Omega_{m0} = 0.26 ~\mathrm{and}~ z_{\mathrm{eq}} = 3135. \tag{25c}
$$

Setting $H_0 = 2.37 \cdot 10^{-4}/\mathrm{Mpc}$ and $k/R_0 = 0.002/\mathrm{Mpc}$ in Eq. (24) we arrive at

$$
N_{\mathrm{HI*}} \simeq 22.6 + \frac{2}{3} \ln \frac{V_{\mathrm{HI0}}^{1/4}}{1~\mathrm{GeV}} + \frac{1}{3} \ln \frac{T_{\mathrm{rh}}}{1~\mathrm{GeV}}. \tag{26}
$$

Throughout our investigation we take $T_{\mathrm{rh}} \simeq 10^9$ GeV as in the majority of these models [3, 10, 14] saturating conservatively the gravitino constraint [34]. This choice for T_{rh} does not affect crucially our results, since T_{rh} appears in Eq. (26) under its logarithm raised to the one third power and therefore, its variation over two or three orders of magnitude has a minor influence on the final value of $N_{\mathrm{HI*}}$.

(ii) The power spectrum of the curvature perturbations given by Eq. (22) is to be confronted with the WMAP7 data [11]:

$$\Delta_{\mathcal{R}} \simeq 4.93 \cdot 10^{-5} \text{ at } k_* = 0.002/\text{Mpc}. \tag{27}$$

(iii) According to the fitting of the WMAP7 results by the cosmological model ΛCDM, n_{s} at the pivot scale $k_* = 0.002/\text{Mpc}$ has to fall within the following range of values [11]:

$$n_{\text{s}} = 0.968 \pm 0.024 \;\Rightarrow\; 0.944 \lesssim n_{\text{s}} \lesssim 0.992 \text{ at } 95\% \text{ c.l.} \tag{28}$$

(iv) Limiting ourselves to a_{s}'s consistent with the assumptions of the power-law ΛCDM cosmological model, we have to ensure that $|a_{\text{s}}|$ remains negligible. Since, within the cosmological models with running spectral index, $|a_{\text{s}}|$'s of order 0.01 are encountered [11], we impose the following upper bound:

$$|a_{\text{s}}| \ll 0.01. \tag{29}$$

3.3 THEORETICAL CONSIDERATIONS

From a more theoretical point of view, the models of (hilltop) FHI can be better refined using the following criteria:

(i) Gauge coupling unification. When G contains non-abelian factors (beyond the SM one), the mass, gv_G, of the lightest gauge boson at the SUSY vacuum, Eq. (8) is to take the value dictated by the unification of the gauge coupling constants within MSSM, i.e.,

$$gv_G \simeq 2 \cdot 10^{16} \text{ GeV } \Rightarrow v_G \simeq 2.86 \cdot 10^{16} \text{ GeV with } g \simeq 0.7, \tag{30}$$

being the value of the unified gauge coupling constant. However, we display in the following results for standard FHI which do not fulfill Eq. (30). This is allowed since the relevant restriction can be evaded if G includes only abelian factors (beyond the SM one) which do not disturb the gauge coupling unification. Otherwise, threshold corrections may be taken into account in order to restore the unification.

(ii) Boundness of V_{HI}. The inflationary potential is expected to be bounded from below. This requirement lets open the possibility that the inflaton may give rise to an inflationary expansion under generic initial conditions set at $\sigma \simeq m_{\text{P}}$.

(iii) Convergence of V_{HI}. The expression of V_{HI} in Eq. (15) is expected to converge at least for $\sigma \sim \sigma_*$. This fact can be ensured if, for $\sigma \sim \sigma_*$, each successive term in the expansion of V_{SUGRA} (and K) Eq. (13) (and Eq. (12)) is smaller than the previous one. In practice, this objective can be easily accomplished if the k's in Eq. (12) – or Eq. (15) – are sufficiently low.

(iv) Monotonicity of V_{HI}. Depending on the values of the coefficients k's in Eq. (15), V_{HI} is a monotonic function of σ or develops a local minimum and maximum. The latter case leads to the possible complication in which the system gets trapped near the minimum of the inflationary potential and, consequently, no FHI takes place. It is, therefore, crucial to check if we can avoid the minimum-maximum structure of V_{HI}. In such a case the system can start its slow rolling from any point on the inflationary path without the danger of getting trapped. This can be achieved, if we require that V_{HI} is a monotonically increasing function of σ, i.e. $V'_{\mathrm{HI}} > 0$ for any σ or, equivalently,

$$V'_{\mathrm{HI}}(\bar{\sigma}_{\min}) > 0 \ \ \text{with} \ \ V''_{\mathrm{HI}}(\bar{\sigma}_{\min}) = 0 \ \ \text{and} \ \ V'''_{\mathrm{HI}}(\bar{\sigma}_{\min}) > 0 \tag{31}$$

where $\bar{\sigma}_{\min}$ is the value of σ at which the minimum of V'_{HI} lies.

(v) Tuning of the initial conditions. When hilltop FHI occurs with σ rolling from the region of the maximum down to smaller values, a mild tuning of the initial conditions is required [22] in order to obtain acceptable n_{s}'s. In particular, the lower n_{s} we want to obtain, the closer we must set σ_* to $\sigma_{\max}$, where $\sigma_{\max}$ is the value of σ at which the maximum of V_{HI} lies. To quantify somehow the amount of this tuning in the initial conditions, we define [22] the quantity:

$$\Delta_{\mathrm{m}*} = \left(\sigma_{\max} - \sigma_*\right)/\sigma_{\max}. \tag{32}$$

The naturalness of the attainment of FHI increases with $\Delta_{\mathrm{m}*}$.

4 FHI IN mSUGRA

The simplest choice of Kähler potential emerging from the expression of Eq. (12) is the one which assures canonical kinetic terms for the inflaton field, S, with the minimal number of terms. This choice is specified in Sec. 4.1 and our results are discussed in Sec. 4.2.

4.1 THE RELEVANT SET-UP

The used Kähler potential in this case can be derived from Eq. (12) by setting:

$$\widehat{K} = 0, \ \widehat{Z} = 1 \ \text{and} \ k_{4S} = k_{6S} = k_{8S} = k_{10S} = k_{12S} = 0. \tag{33}$$

Upon substituting Eqs. (14a) – (14f) into Eq. (15) we infer that the resulting V_{HI} takes the form

$$V_{\mathrm{HI}} \simeq V_{\mathrm{HI0}} \left(1 + c_{\mathrm{HI}} - a_S \frac{\sigma}{\sqrt{2V_{\mathrm{HI0}}}} + \frac{\sigma^4}{8 m_{\mathrm{P}}} \right), \tag{34}$$

since in this case $c_{2K}^{(0)} = 0$ and $c_{4K}^{(0)} = 1/2$. It is worth mentioning that mSUGRA is, in principle, beneficial for the implementation of FHI, since it does not generate any new contribution in the η parameter, Eq. (20), due to a miraculous cancellation emerging in the computation of $c_{2K}^{(0)}$. Despite this fact, fixing all the remaining terms in Eq. (12) beyond the quadratic term equal to zero can be regarded as an ugly tuning.
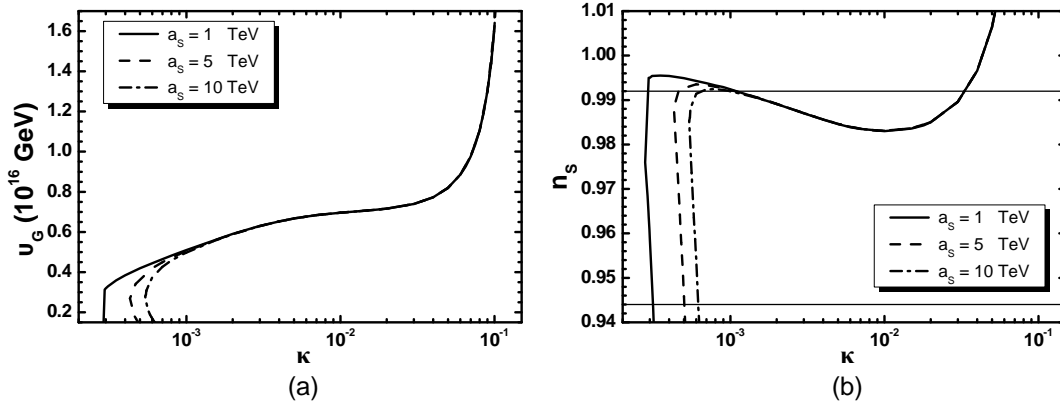
FIGURE 3: *The allowed by Eqs. (26) and (27) values of v_G [n_s] versus κ for standard FHI with $N = 2$ and $a_S = 1$ TeV (solid lines), $a_S = 5$ TeV (dashed lines) and $a_S = 10$ TeV (dot-dashed lines). The region of Eq. (28) is also limited by thin lines.*

4.2 RESULTS

The investigation of this model of FHI depends on the parameters:

$$\sigma_*, v_G, a_S \quad \text{and} \quad \begin{cases} \kappa & \text{for standard and shifted FHI}, \\ M_S & \text{for smooth FHI}, \end{cases}$$

where we fix $M_S = 5 \cdot 10^{17}$ GeV in the case of shifted FHI. In our computation, we use as input parameters a_S and κ or M_S. We then restrict v_G and σ_* so as Eqs. (26) and (27) are fulfilled. Using Eqs. (23a) and (23b) we can extract n_s and α_s respectively. Our findings for standard [shifted and smooth] FHI are displayed in Sec. 4.2.1 [Sec. 4.2.2].

We can obtain a rather accurate estimation of the expected n_s's if we omit the third term in the r.h.s of Eq. (34), calculate analytically the integral in Eq. (19), replace the σ_f's by their values in Eq. (21) and solve the resulting equation w.r.t σ_*. Taking into account that $\epsilon < \eta$ we can extract n_s from Eq. (23a) and find

$$n_s \simeq \begin{cases} 1 - 1/N_{\text{HI}*} + 3\kappa^2 N N_{\text{HI}*}/4\pi^2 & \text{for standard FHI}, \\ 1 - 1/N_{\text{HI}*} + 3\kappa^2 N_{\text{HI}*}/2\pi^2 & \text{for shifted FHI}, \\ 1 - 5/3N_{\text{HI}*} + 2\left(6\mu_S^2 M_S^2 N_{\text{HI}*}/m_P^4\right)^{1/3} & \text{for smooth FHI}. \end{cases} \quad (35)$$

Observing that the last term in the r.h.s of the expressions above arise from the last term in the r.h.s of Eq. (34), we can easily infer that mSUGRA increases significantly n_s for relatively large κ's or M_S's.

On the other hand, the third term in the r.h.s of Eq. (34) can be important for $\kappa \leq 6 \cdot 10^{-4}$ and $M \leq 10^{15}$ GeV – cf. Ref. [14]– since it becomes comparable with the second term there. In this regime, the required by Eq. (26) σ_* becomes comparable to σ_c and the

approximation of $f_{\rm rc}$ in Eq. (18) is no longer valid. Instead, we here have

$$f_{\rm rc}(x) = 3 - \frac{x^{-2}}{6} - \frac{x^{-4}}{30} - \frac{x^{-6}}{84} - \frac{x^{-8}}{180} - \frac{x^{-10}}{330} - \frac{x^{-12}}{546} - \frac{x^{-14}}{840} - \frac{x^{-16}}{1224} - \frac{x^{-18}}{1710} - \frac{x^{-20}}{2310} - \cdots$$

(36)

As a consequence, $V'_{\rm HI}$ decreases sharply (enhancing $N_{\rm HI*}$) whereas $|V''_{\rm HI}|$ (or η) increases adequately, lowering thereby $n_{\rm s}$ to an acceptable level.

4.2.1 STANDARD FHI

In the case of standard FHI (with $\mathsf{N} = 2$), we display in Fig. 3-(a) the allowed by Eqs. (26) and (27) values of v_G versus κ. The corresponding variation of $n_{\rm s}$ versus κ is depicted in Fig. 3-(b) where the observationally compatible region of Eq. (28) is also delimited by thin lines. Solid, dashed and dot-dashed lines stand for the results obtained for $\mathrm{a}_S = 1, 5$ and 10 TeV respectively. We observe that the various lines coincide for $\kappa \gtrsim 6 \cdot 10^{-4}$. For the sake of clarity we do not show in Fig. 3 solutions with $v_G > 2 \cdot 10^{16}$ GeV or $\kappa < 2 \cdot 10^{-4}$ – cf. Ref. [14] – which are totally excluded by Eq. (28). The third [last] term in the r.h.s of Eq. (34) become important for $\kappa \gtrsim 0.01$ [$\kappa \lesssim 6 \cdot 10^{-4}$] whereas for $6 \cdot 10^{-4} \lesssim \kappa \lesssim 0.01$, the second term in the r.h.s of Eq. (34) becomes prominent. As a consequence, the last term in the r.h.s of Eq. (34) drives $n_{\rm s}$ to values close to or larger than unity whereas the third one succeed in reconciling it with Eq. (28) for discriminated κ's related to the chosen a_S's. Namely, from Fig. 3 we deduce that there is a marginally allowed area for

$$0.0015 \lesssim \kappa \lesssim 0.032, \quad 5.5 \lesssim v_G/(10^{15} \text{ GeV}) \lesssim 7.5, \tag{37a}$$

$$0.983 \lesssim n_{\rm s} \lesssim 0.99 \ \text{ and } \ 1.2 \lesssim |\alpha_{\rm s}|/10^{-4} \lesssim 3.5. \tag{37b}$$

In addition, from Fig. 3 we find isolated corridors consistent with Eq. (28), e.g.

$$\kappa \simeq 3 \cdot 10^{-4}, \ 5 \cdot 10^{-4}, \ 6 \cdot 10^{-4} \ \text{ with } \ v_G \lesssim 3 \cdot 10^{15} \text{ GeV for } \mathrm{a}_S = 1, 5 \text{ and } 10 \text{ TeV}, \tag{37c}$$

respectively. We remark that the v_G's allowed here lie well below the ones required by Eq. (30). In conclusion, although standard FHI in mSUGRA can not be excluded, it can be considered as rather disfavored since the allowed region is extremely limited.

4.2.2 SHIFTED AND SMOOTH FHI

In the cases of shifted and smooth FHI we confine ourselves to the values of the parameters consistent with Eq. (30) and display the solutions fulfilling Eqs. (26) and (27) in Table 1. Given that $\mathrm{a}_S \sim 1$ TeV plays no role in the determination of the inflationary observables, we conclude that the resulting $n_{\rm s}$'s and $\alpha_{\rm s}$'s are obviously predictions of these FHI models – without the possibility of altering them by some adjustment. We observe that the required κ, in the case of shifted FHI, is rather low and so, the last terms in the r.h.s of Eq. (34) is more or less negligible. As a result, η is exclusively determined by $c_{\rm HI} V_{\rm HI0}$ and $n_{\rm s}$ remains within the range of Eq. (28) although outside the 68% c.l. region. On the contrary, in the case of smooth FHI, η strongly depends on the last term in the r.h.s of Eq. (34) enhancing thereby $n_{\rm s}$ beyond the range of Eq. (28). In the latter case, $|\alpha_{\rm s}|$ is also considerably enhanced.

Shifted FHI		Smooth FHI	
$\kappa/10^{-3}$	9.2	$M_{\rm S}/5 \cdot 10^{17}$ GeV	0.79
$\sigma_*/10^{16}$ GeV	5.37	$\sigma_*/10^{16}$ GeV	32.9
$M/10^{16}$ GeV	2.3	$\mu_{\rm S}/10^{16}$ GeV	0.21
$1/\xi$	4.36	$\sigma_{\rm f}/10^{16}$ GeV	13.4
$N_{\rm HI*}$	52.2	$N_{\rm HI*}$	53
$n_{\rm s}$	0.982	$n_{\rm s}$	1.04
$-\alpha_{\rm s}/10^{-4}$	3.4	$-\alpha_{\rm s}/10^{-4}$	16.6

TABLE 1: *Input and output parameters consistent with Eqs. (26), (27) and (30) for shifted (with $M_{\rm S} = 5 \cdot 10^{17}$ GeV) or smooth FHI within mSUGRA.*

5 HILLTOP FHI IN nmSUGRA

The fitting of the WMAP7 data with the ΛCDM model enforces [22, 23] us to consider more complicated (and possibly more general) forms of Kälher potentials. The simplest choice is to consider of a moderate deviation from mSUGRA, named [22] nmSUGRA, according to which the next-to-minimal term is tuned so as an adequately small, negative mass squared for the inflaton is generated. This setting is outlined in Sec. 5.1 and the structure of the resulting $V_{\rm HI}$ is analyzed in Sec. 5.2. Our results are exhibited in Sec. 5.3.

5.1 THE RELEVANT SET-UP

In this scenario, the form of the relevant Kähler potential is given by Eq. (12), setting

$$\widehat{K} = k_{6S} = k_{8S} = k_{10S} = k_{12S} = 0 \ \text{ and } \ \widehat{Z} = 1. \tag{38a}$$

Therefore, $V_{\rm HI}$ takes the form of Eq. (15) with

$$c_{2K} = c_{2K}^{(0)} = k_{4S}, \ c_{4K} = c_{4K}^{(0)}(k_{6S} = 0) \ \text{ and } \ c_{2\nu K} = 0 \ \text{ for } \ \nu \geq 3. \tag{38b}$$

Note that the expansion of $V_{\rm SUGRA}$ in Eq. (13) terminates at the terms of order $|S|^4$ consistently with the fact that the expansion of K terminates at the terms of order $|S|^6$.
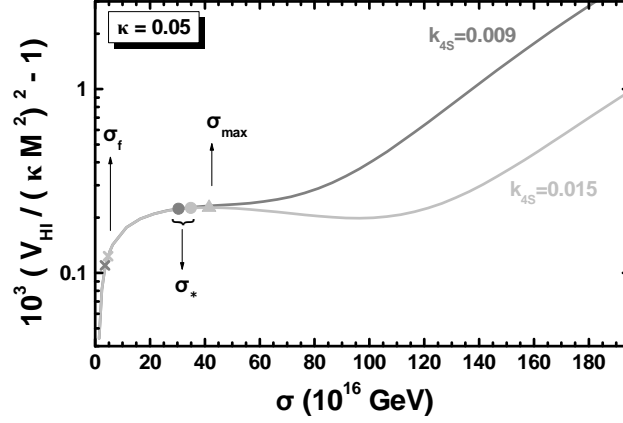
5.2 STRUCTURE OF THE INFLATIONARY POTENTIAL

For σ close to σ_*, $V_{\rm HI}$ given by Eq. (15) can be approximated as

$$V_{\rm HI} \simeq V_{\rm HI0} \left(1 + c_{\rm HI} - k_{4S}\frac{\sigma^2}{2m_{\rm P}^2} + c_{4K}\frac{\sigma^4}{4m_{\rm P}^4} \right). \tag{39}$$

Given that $c_{4K} = c_{4K}^{(0)} \simeq 1/2$ is much larger than k_{4S}, the boundedness of $V_{\rm HI}$ is ensured in this scenario, by construction.

FIGURE 4: *The variation of V_{HI} in Eq. (39) as a function of σ for standard FHI in nmSUGRA, $\kappa = 0.05$ and $k_{4S} = 0.009$ ($n_s = 0.968$) [$k_{4S} = 0.015$ ($n_s = 0.944$)](gray [light gray] line). The values of σ_*, σ_f and σ_{max} are also depicted.*

The monotonicity of V_{HI} in Eq. (39) can be investigated applying Eq. (31). In particular, we can find approximately – note that in the formulas below, we have $c_{4K} \simeq 1/2$:

$$\bar{\sigma}_{\min} \simeq \begin{cases} \sqrt{k_{4S}/3c_{4K}}\ m_P & \text{for standard and shifted FHI,} \\ \sqrt{2m_P/3}\left(\sqrt{5/2c_{4K}}\ \mu_S M_S\right)^{1/4} & \text{for smooth FHI.} \end{cases} \tag{40}$$

Inserting Eq. (40) into Eq. (31), we find that V_{HI} remains monotonic for

$$k_{4S} < k_{4S}^{\max} \text{ with } k_{4S}^{\max} = \begin{cases} 3\kappa\sqrt{c_{4K}\mathsf{N}}/4\pi & \text{for standard FHI,} \\ 3\kappa\sqrt{c_{4K}}/2\sqrt{2}\pi & \text{for shifted FHI,} \\ (8/3)(2c_{4K}/5)^{3/4}\sqrt{\mu_S M_S}/m_P & \text{for smooth FHI.} \end{cases} \tag{41}$$

For $k_{4S} > k_{4S}^{\max}$, V_{HI} reaches a local minimum [maximum] at the inflaton-field value $\sigma_{\min}$ [$\sigma_{\max}$] which can be estimated as follows:

$$\sigma_{\min} \simeq \sqrt{\frac{k_{4S}}{c_{4K}}}m_P \text{ and } \sigma_{\max} \simeq \begin{cases} \kappa m_P\sqrt{\mathsf{N}}/2\sqrt{2k_{4S}}\pi & \text{for standard FHI,} \\ \kappa m_P/2\sqrt{k_{4S}}\pi & \text{for shifted FHI,} \\ \sqrt{2/3}\sqrt[3]{k_{4S}}(\mu_S M_S m_P)^{1/3} & \text{for smooth FHI.} \end{cases} \tag{42}$$

The structure of V_{HI} is depicted in Fig. 4 where we display V_{HI} as a function of σ for standard FHI in nmSUGRA, $\kappa = 0.05$ and $k_{4S} = 0.009$ (gray line) or $k_{4S} = 0.015$ (light gray line). In the first case (gray line) we obtain $n_s = 0.968$ with $k_{4S} < k_{4S}^{\max} \simeq 0.011$ and therefore V_{HI} remains monotonic. On the contrary, for $k_{4S} = 0.015$ we get $n_s = 0.944$ with $k_{4S} > k_{4S}^{\max}$ and therefore V_{HI} develops the minimum-maximum structure with the maximum being located at $\sigma_{\max} = 4.15 \cdot 10^{17}$ GeV. The resulting Δ_{m*} in the latter case is $\Delta_{m*} = 0.16$. The values of σ_* and σ_f are also depicted.
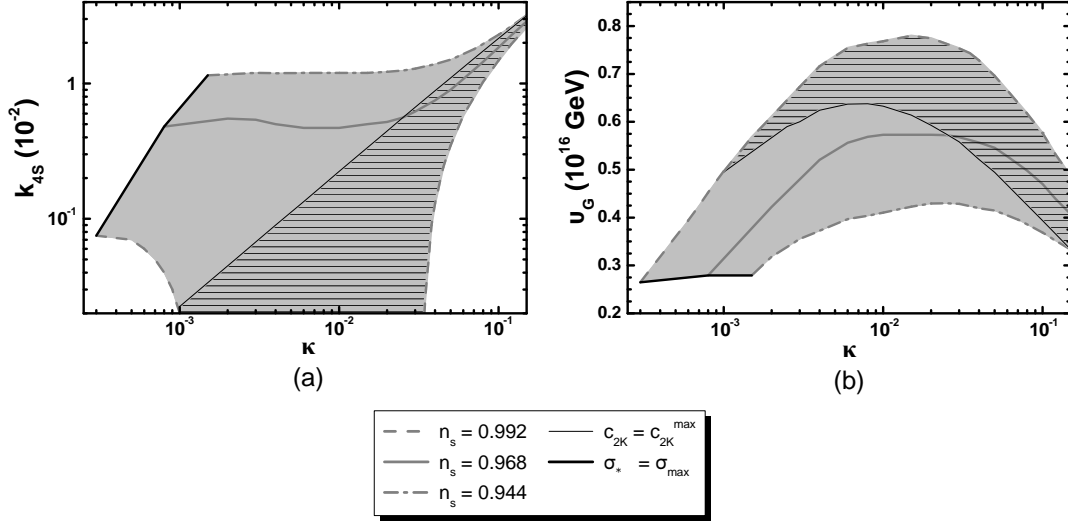
FIGURE 5: *Allowed (lightly gray shaded) region as determined by Eqs. (26)-(29) in the $\kappa - c_{2K}$ [$\kappa - v_G$] plane (a) [(b)] for standard FHI within the nmSUGRA. Ruled are the regions where the inflationary potential remains monotonic. The conventions adopted for the various lines are also shown.*

5.3   RESULTS

Our strategy in the numerical investigation of the nmSUGRA scenario is the one described in Sec. 4.2 – recall that we fix $a_S = 1$ TeV henceforth and no impact from that term on our results is detected. In addition to the parameters manipulated there, we have here the parameter k_{4S} which can be adjusted so as to achieve n_s in the range of Eq. (28). We check also the fulfillment of Eq. (31). Our findings for standard [shifted and smooth] FHI are accommodated in Sec. 5.3.1 [Sec. 5.3.2].

Employing the procedure outlined in Sec. 4.2 above Eq. (35) we can take a flavor for the expected n_s's in the nmSUGRA scenario, for any k_{4S}:

$$
n_s \simeq \begin{cases} 1 - 2k_{4S}\left(1 - 1/c_N\right) - 6c_{4K}\kappa^2 \mathsf{N}c_N/4k_{4S}\pi^2 & \text{for standard FHI,} \\ 1 - 2k_{4S}\left(1 - 1/c_N\right) - 6c_{4K}\kappa^2 c_N/2k_{4S}\pi^2 & \text{for shifted FHI,} \\ 1 - 5/3N_{\mathrm{HI*}} + 2\tilde{c}_N - \left(2\tilde{c}_N N_{\mathrm{HI*}} + 7\right)k_{4S} & \text{for smooth FHI,} \end{cases} \tag{43}
$$

with $c_N = 1 - \sqrt{1 + 4k_{4S}N_{\mathrm{HI*}}}$ and $\tilde{c}_N = 2c_{4K}\left(6\mu_S^2 M_S^2 N_{\mathrm{HI*}}/m_{\mathrm{P}}^4\right)^{1/3}$.

We can clearly appreciate the contribution of a positive k_{4S} in lowering of n_s.

5.3.1   STANDARD FHI

In the case of standard FHI (with $\mathsf{N} = 2$), we delineate the (lightly gray shaded) region allowed by Eqs. (26)-(29) in the $\kappa - k_{4S}$ [$\kappa - v_G$] plane – see Fig. 5-(a) [Fig. 5-(b)]. The

SHIFTED FHI				SMOOTH FHI			
$n_{\rm s}$	0.944	0.968	0.992	$n_{\rm s}$	0.944	0.968	0.992
$k_{4S}/10^{-3}$	11.7	4.5	-3.2	$k_{4S}/10^{-3}$	9.65	7.6	5.4
$k_{4S}^{\rm max}/10^{-3}$	1.8	1.9	2.2	$k_{4S}^{\rm max}/10^{-3}$	9.1	9.2	9.2
$\Delta_{\rm m*}/10^{-2}$	16	39	$-$	$\Delta_{\rm m*}/10^{-2}$	7	$-$	$-$
$\sigma_*/10^{16}$ GeV	2.45	3.1	4.31	$\sigma_*/10^{16}$ GeV	23.8	24.9	26.6
$\kappa/10^{-3}$	8.1	8.7	9.7	$M_{\rm S}/5 \cdot 10^{17}$ GeV	2.4	1.83	1.4
$M/10^{16}$ GeV	2.2	2.26	2.3	$\mu_{\rm S}/10^{16}$ GeV	0.07	0.09	0.12
$1/\xi$	4.1	4.3	4.5	$\sigma_{\rm f}/10^{16}$ GeV	13.4	13.4	13.4
$N_{\rm HI*}$	51.9	52.1	52.3	$N_{\rm HI*}$	52.3	52.4	52.6
$-\alpha_{\rm s}/10^{-4}$	3.1	3.5	3.5	$-\alpha_{\rm s}/10^{-3}$	0.7	0.9	1.1

TABLE 2: *Input and output parameters consistent with Eqs. (26) - (30) for shifted (with $M_{\rm S} = 5 \cdot 10^{17}$ GeV) or smooth FHI in nmSUGRA.*

conventions adopted for the various lines are also shown. In particular, the dashed [dot-dashed] lines correspond to $n_{\rm s} = 0.992$ [$n_{\rm s} = 0.944$], whereas the gray solid lines are obtained by fixing $n_{\rm s} = 0.968$ – see Eq. (28). Below the black solid lines, our initial assumption $\sigma_* < \sigma_{\rm max}$ is violated. In the hatched regions, Eq. (31) is also satisfied and along their boundaries designed by thin, black, solid lines Eq. (41) is saturated. We observe that the optimistic constraint of Eq. (31) can be met in a rather wide fraction of the allowed area. In particular, for $n_{\rm s} = 0.968$ we find

$$\{0.8\}\ 2.5 \lesssim \frac{\kappa}{10^{-2}} \lesssim 15, \ \ \{11\}\ 5.7 \gtrsim \frac{v_G}{10^{15}\ \text{GeV}} \gtrsim 4.1, \tag{44a}$$

$$\{0.48\}\ 0.56 \lesssim \frac{k_{4S}}{10^{-2}} \lesssim 2.9 \ \text{and} \ \{0.2\}\ 0.39 \lesssim -\frac{\alpha_{\rm s}}{10^{-3}} \lesssim 1.1, \tag{44b}$$

where the limiting values obtained without imposing Eq. (31) are indicated in curly brackets. In the corresponding region, $\Delta_{\rm m*}$ ranges between 0 and 50%. Note that the v_G's encountered here are lower that those required by Eq. (30).

5.3.2 SHIFTED AND SMOOTH FHI

In the cases of shifted and smooth FHI we confine ourselves to the values of the parameters which satisfy Eq. (30) and display in Table 2 their values which are consistent with Eqs. (26)-(29) as well. In the case of shifted FHI, we observe that (i) we need positive k_{4S} to obtain $n_{\rm s} = 0.992$ since the mSUGRA result is lower – see Table 1; (ii) the lowest possible $n_{\rm s}$ compatible with the conditions of Eq. (31) is 0.976 and so, $n_{\rm s} = 0.968$ is not consistent with Eq. (31). In the case of smooth FHI, we see that a reduction of $n_{\rm s}$ consistently with Eq. (31) can be achieved for $n_{\rm s} \gtrsim 0.951$ and so $n_{\rm s} = 0.968$ can be obtained without complications.

6 HILLTOP FHI IN nnmSUGRA

Another possible SUGRA set-up which can accommodate an observationally viable FHI is the one, first proposed in Ref. [25], which we here name nnmSUGRA. In this case, a convenient choice, specified in Sec. 6.1, of the next-to-minimal and the next-to-next-to-minimal terms in the Kähler potential is employed. The structure of the resulting $V_{\rm HI}$ is studied in Sec. 6.2 and our related results are exhibited in Sec. 6.2.

6.1 THE RELEVANT SET-UP

In this scenario, the form of the relevant Kähler potential is given by Eq. (12) after setting

$$\widehat{K} = 0 \ \text{ and } \ \widehat{Z} = 1 \tag{45a}$$

and so $V_{\rm HI}$ takes the form of Eq. (15) with

$$c_{2K} = c_{2K}^{(0)} = k_{4S}, \ \ c_{4K} = c_{4K}^{(0)}, \ \ c_{6K} = c_{6K}^{(0)}, \ \ c_{8K} = c_{8K}^{(0)} \ \text{ and } \ c_{10K} = c_{10K}^{(0)}. \tag{45b}$$

In other words, this scenario is the most general one which arises from the Kähler potential of Eq. (12) in the absence of h_m's. The crucial difference between nnmSUGRA and nmSUGRA, however is the sign of $c_{2K} = k_{4S}$ which is here negative. As a consequence, fulfilling of Eq. (28) requires negative c_{4K} or positive k_{6S} – see Eq. (14d). The inclusion of higher order terms in the expansion of Eq. (13) prevents the runaway behavior of the resulting $V_{\rm HI}$ – see Eq. (15).

6.2 STRUCTURE OF THE INFLATIONARY POTENTIAL

For σ close to σ_*, $V_{\rm HI}$ given by Eq. (15) can be approximated as

$$V_{\rm HI} \simeq V_{\rm HI0} \left(1 + c_{\rm HI} - k_{4S}\frac{\sigma^2}{2m_{\rm P}^2} + c_{4K}\frac{\sigma^4}{4m_{\rm P}^4} - c_{6K}\frac{\sigma^6}{8m_{\rm P}^6} \right). \tag{46}$$

The monotonicity of $V_{\rm HI}$ here can be checked only numerically – due to the numerous terms involved in $V_{\rm HI}'$ and $V_{\rm HI}''$ – by applying the criterion in Eq. (31). In the case of a non-monotonic $V_{\rm HI}$, we can show that it reaches a local maximum at the inflaton-field value:

$$\sigma_{\max} \simeq \begin{cases} \dfrac{m_{\rm P}\sqrt{2\pi|k_{4S}|+\sqrt{2}\sqrt{2k_{4S}^2\pi^2+{\rm N}k^2|c_{4K}|}}}{2\sqrt{\pi|c_{4K}|}} & \text{for standard FHI,} \\ \dfrac{m_{\rm P}\sqrt{\pi|k_{4S}|+\sqrt{k_{4S}^2\pi^2+k^2|c_{4K}|}}}{\sqrt{2\pi|c_{4K}|}} & \text{for shifted FHI,} \\ (2/3)^{3/8}\sqrt{m_{\rm P}\sqrt{\mu_{\rm S}\overline{M}_{\rm S}}}/|c_{8K}|^{1/8} & \text{for smooth FHI.} \end{cases} \tag{47}$$

and a local minimum at the inflaton-field value:

$$\sigma_{\min} \simeq m_{\rm P}\frac{\sqrt{-3|c_{6K}| + \sqrt{9c_{6K}^2 + 32|c_{4K}c_{6K}|}}}{2\sqrt{|c_{8K}|}}. \tag{48}$$
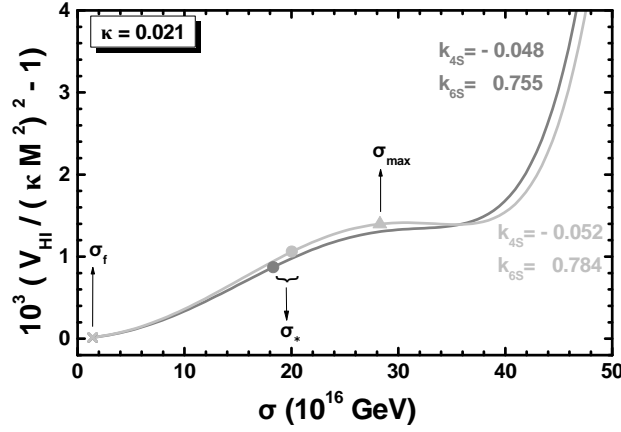
FIGURE 6: *The variation of V_{HI} in Eq. (46) as a function of σ for standard FHI in nnmSUGRA, $\kappa = 0.021$, $k_{8S} = -1.5, k_{10S} = -1, k_{12S} = 0.5$ and $k_{4S} = -0.048, k_{6S} = 0.755$ ($n_s = 0.968$) [$k_{4S} = -0.052, k_{6S} = 0.784$ ($n_s = 0.944$)] (gray [light gray] line). The values of σ_*, σ_f and σ_{max} are also depicted.*

The last result holds for all the types of FHI, since for σ's close σ_{min}, V_{HI} is dominated by the last terms of the expansion in the r.h.s of Eq. (15) and so, any depedence on c_{HI}, which essentially indentifies the type of FHI, is switched off.

The structure of V_{HI} is depicted in Fig. 6 where we display V_{HI} as a function of σ for standard FHI in nnmSUGRA, $\kappa = 0.021, k_{8S} = -1.5, k_{10S} = -1, k_{12S} = 0.5$ and $k_{4S} = -0.048, k_{6S} = 0.755$ (gray line) or $k_{4S} = -0.052, k_{6S} = 0.784$ (light gray line). In the first case (gray line) we obtain $n_s = 0.968$ and V_{HI} remains monotonic. On the contrary, in the second case (light gray line) V_{HI} develops the minimum-maximum structure and we get $n_s = 0.944$. The maximum of V_{HI} is located at $\sigma_{max} = 2.8 \cdot 10^{17}$ GeV and we get $\Delta_{m*} = 0.29$. The values of σ_* and σ_f are also depicted.

6.3 RESULTS

Our strategy in the numerical investigation of the nnmSUGRA scenario is the one described in Sec. 4.2. In addition to the parameters manipulated there, we have here the parameters k_{4S} and k_{6S} which can be adjusted in order to fulfill Eq. (28) whereas the boundedness of V_{HI} is controlled by the $k_{2\nu S}$'s with $4 \leq \nu \leq 6$. We check also the validity of Eq. (31). Our findings for standard [shifted and smooth] FHI are arranged in Sec. 6.3.1 [Sec. 6.3.2].

Preliminarily results on the n_s's expected, however, can be extracted by applying the procedure highlighted above Eq. (35). Namely, for standard FHI we find

$$n_s \simeq 1 - \frac{1}{2}\left(2|k_{4S}| + \frac{1}{\pi}\left(3\sqrt{4\Delta_{1K}}\tanh\frac{N_{HI*}\sqrt{\Delta_{1K}}}{\pi} + \operatorname{arctanh}\frac{\Delta_{2K}\pi}{\sqrt{\Delta_{1K}}}\right)\right) \quad (49a)$$

where

$$\Delta_{1K} = (|c_{4K}|k^2 N + 2k_{4S}^2\pi^2)/2 \ \text{ and } \ \Delta_{2K} = -4|c_{4K}|M^2/m_P^2 + |k_{4S}|. \quad (49b)$$
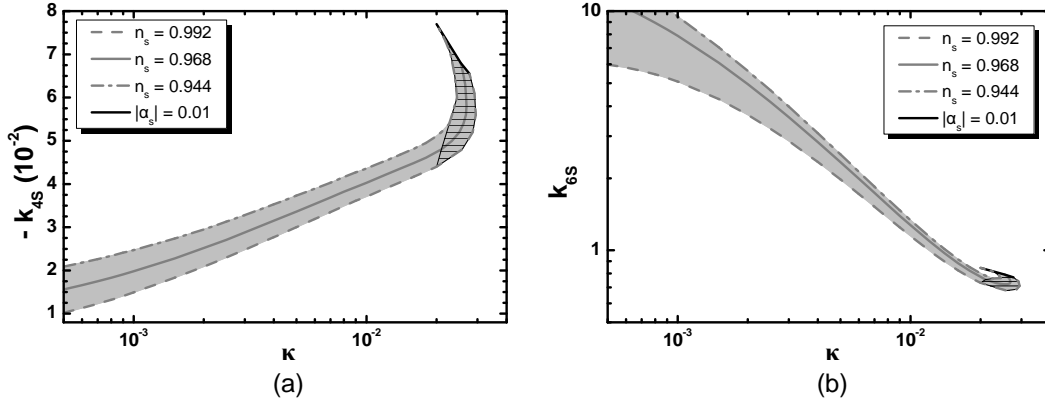
FIGURE 7: *Allowed (lightly gray shaded) region, as determined by Eqs. (26)-(30), in the $\kappa - (-k_{4S})$ [$\kappa - k_{6S}$] plane (a) [(b)] for standard FHI in nnmSUGRA. We take $k_{8S} = -1.5, k_{10S} = -1$ and $k_{12S} = 0.5$. Hatched are the regions where V_{HI} remains monotonic. The conventions adopted for the various lines are also shown.*

The result for shifted FHI can be obtained from the expression above setting $N = 2$ and replacing 4 with 2 in the formula of Δ_{2K} in Eq. (49b). We did not succeed to obtain similar formulas for smooth FHI due to complications related to the numerus significant terms in V_{HI}, Eq. (46).

6.3.1 STANDARD FHI

One of the outstanding advantages of the realization of standard FHI within nnmSUGRA is that Eq. (30) can be attained – cf. Figs. 3-(a), 5-(b) and 11-(b), below. Therefore, in this scenario, we are able to display regions (lightly gray shaded) allowed by Eqs. (26) – (30) in the $\kappa - (-k_{4S})$ [$\kappa - k_{6S}$] plane – see Fig. 7-(a) [Fig. 7-(b)] – for $k_{8S} = -1.5, k_{10S} = -1, k_{12S} = 0.5$. The conventions adopted for the various lines are also shown. In particular, the gray dashed [dot-dashed] lines correspond to $n_s = 0.992$ [$n_s = 0.944$], whereas the gray solid lines have been obtained by fixing $n_s = 0.968$ – see Eq. (28). We remark that increasing $|k_{4S}|$'s the required k_{6S}'s drop. We observe that the optimistic constraint of Eq. (31) can be met in a very limited slice of the allowed area. In this region also σ_* turns out to be rather large ($\sim 10^{17}$ GeV) and therefore we observe a mild dependence of our results on c_{6K} (or k_{8S}) too. Also there is a remarkable augmentation of α_s which saturates the bound of Eq. (29) along the thick black solid line. Namely, for $n_s = 0.968$ we find

$$\{0.05\}\ 2.1 \lesssim \frac{\kappa}{10^{-2}} \lesssim 2.5, \quad \{1.5\}\ 4.8 \lesssim \frac{-k_{4S}}{10^{-2}} \lesssim 6.8 \tag{50a}$$

$$7.2 \lesssim \frac{k_{6S}}{10^{-1}} \lesssim 7.55\ \{11.2\} \quad \text{and} \quad \{1.5 \cdot 10^{-3}\}\ 0.48 \lesssim -\frac{\alpha_s}{10^{-2}} \lesssim 1, \tag{50b}$$

where the limiting values obtained without imposing Eq. (31) are indicated in curly brackets. In the corresponding region, Δ_{m*} ranges between 18 and 38%. As can be deduced from Fig. 7-(a), Δ_{m*} increases with $|k_{4S}|$ or as k_{6S} drops.
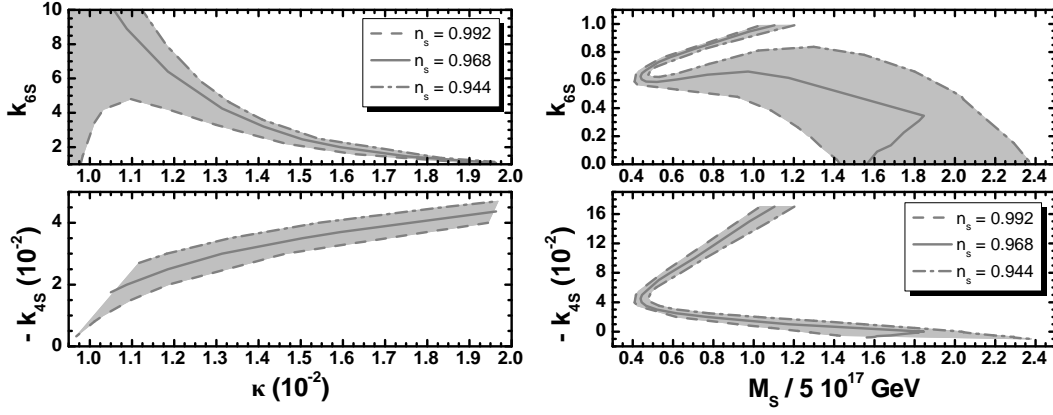
FIGURE 8: *Allowed (lightly gray shaded) regions, as determined by Eqs. (26)-(30), in the $\kappa - (-k_{4S})$ and $\kappa - k_{6S}$ planes for shifted FHI (left graphs) or in the $M_S - (-k_{4S})$ and $M_S - k_{6S}$ planes for smooth FHI (right graphs) in nnmSUGRA. We take $k_{8S} = -1.5, k_{10S} = -1$ and $k_{12S} = 0.5$. The conventions adopted for the various lines are also shown.*

6.3.2   SHIFTED AND SMOOTH FHI

As in the other scenaria, shifted and smooth FHI can become consistent with Eq. (30). Contrary to the the other scenaria, though, the consideration of two parameters (k_{4S} and k_{6S}) allows here to find wider regions of parameters compatible with Eqs. (26)-(30). These are shown in Fig. 8 for shifted [smooth] FHI, $k_{8S} = -1.5, k_{10S} = -1$ and $k_{12S} = 0.5$ (left [right] panel). The solid, dashed and dot-dashed gray lines correspond, as usual, to $n_s = 0.968, 0.992$ and 0.944 respectively. More specifically,

- In the case of shifted FHI, we display the allowed regions in the $\kappa - (-k_{4S})$ and $\kappa - k_{6S}$ planes. The left and right boundaries of the allowed regions come from the bounds on ξ – see Sec. 2.1. The results are pretty stable against variations of k_{8S} since the used κ's are rather low whereas Eq. (31) is violated throughout. For $n_s = 0.968$ we obtain $\Delta_{m*} \simeq 0.29 - 0.33$ and $\alpha_s \simeq (1.2 - 5.7) \cdot 10^{-3}$ with

$$1.05 \lesssim \kappa/10^{-2} \lesssim 1.96, \quad 1.7 \lesssim -k_{4S}/10^{-2} \lesssim 4 \text{ and } 1.1 \gtrsim k_{6S} \gtrsim 10. \quad \text{(51a)}$$

- In the case of smooth FHI, we display the allowed areas in the $M_S - (-k_{4S})$ and $M_S - k_{6S}$ planes. It is worth mentioning that V_{HI} remains monotonic almost in the whole allowed region depicted in the graphs. Only minor portions close the dot-dashed line violate Eq. (31). For $n_s = 0.968$ we obtain $0.6 \lesssim |\alpha_s|/10^{-3} \lesssim 8$ with

$$0.4 \lesssim M_S/5 \cdot 10^{17} \text{ GeV} \lesssim 1.82, \quad 0 \lesssim -k_{4S} \lesssim 0.17 \text{ and } 0.3 \lesssim k_{6S} \lesssim 0.99. \quad \text{(51b)}$$

In both cases above we observe that k_{4S} is tuned to rather low values whereas k_{6S} can be adjusted to rather natural values of order one. This naturalness is removed only in a very minor slice of the allowed region where positive k_{4S}'s can be considered and the required k_{6S}'s are tuned to values of order 0.01.

7 HILLTOP FHI IN hSUGRA

Another, more drastic (and perhaps more radical) way to circumvent the n_s problem of FHI is the inclusion of extra fields in K. This proposition [16] is based on the observation that these fields provide extra terms in the expressions of $c_{\nu K}$ in Eq. (13). As a bonus, this construction gives us the opportunity to elude the notorious η problem of FHI. The Kähler potential of these extra field is specified in Eq. (7.1) and the structure of the resulting V_{HI} is studied in Sec. 7.2. Our results are presented in Sec. 7.3.

7.1 THE RELEVANT SET-UP

As we mention in Sec. 2.3, the dependence of K on the h_m's is encoded in the elements $\widehat{K}$ and $\widehat{Z}$. Motivated by several superstring and D-brane models [35], we seek the following ansatz for them:

$$\widehat{K} = m_{\mathrm{P}}^2 \sum_{m=1}^{\mathsf{M}} \beta_m \ln \frac{h_m + h_m^*}{m_{\mathrm{P}}} \ \text{ and } \ \widehat{Z} = k_Z \prod_{m=1}^{\mathsf{M}} \left(\frac{h_m + h_m^*}{m_{\mathrm{P}}} \right)^{\alpha_m} \ \text{ with } \ \beta_m < 0. \quad (52)$$

The last restriction in Eq. (52) is demanded so as to obtain positivity of the various kinetic energies. We further assume that β_m's have to be integers and α_m's have to be rational numbers. Also M measures the number of hidden sector fields. We here restrict ourselves to its lowest possible value, $\mathsf{M} = 1$, defining $\alpha := \alpha_1$ and $\beta := \beta_1$. Note, in passing, that the form used here for $\widehat{K}$ and $\widehat{Z}$ has been initially proposed in Ref. [36] in order to justify the saddle point condition needed for the attainment of A-term or MSSM inflation [37].

In the presence of $\widehat{K}$ and $\widehat{Z}$ in Eq. (52), the coefficients c_{1K} and $c_{2\nu K}$ in the series of Eqs. (13) and (15) receive extra contributions beyond those exposed in Eqs. (14b)–(14f). The total expressions for c_{1K} and $c_{2\nu K}$ are found to be

$$c_{1K} = c_{1K}^{(0)} + \alpha + \beta, \tag{53a}$$

$$c_{2K} = c_{2K}^{(0)} + \frac{(\alpha - \beta)^2}{\beta}, \tag{53b}$$

$$c_{4K} = c_{4K}^{(0)} + \frac{(\alpha - \beta)^3}{\beta^2}, \tag{53c}$$

$$c_{6K} = c_{6K}^{(0)} + \frac{(\alpha - \beta)^2(2\alpha^2 - 2\alpha\beta + \beta^2)}{2\beta^3} - \left(\alpha + \frac{\alpha^3}{2\beta^2} - \frac{5\alpha^2}{4\beta} - \frac{\beta}{4} \right) k_{4S}, \tag{53d}$$

$$\begin{aligned} c_{8K} = \ & c_{8K}^{(0)} + \frac{(\alpha - \beta)^2(6\alpha^3 - 6\alpha^2\beta + 3\alpha\beta^2 - \beta^3)}{6\beta^4} \\ & + \left(\frac{5\alpha}{4} - \frac{\alpha^4}{\beta^3} + \frac{11\alpha^3}{4\beta^2} - \frac{11\alpha^2}{4\beta} - \frac{\beta}{4} \right) k_{4S} \\ & + \left(\frac{5\alpha}{6} + \frac{\alpha^3}{2\beta^2} - \frac{7\alpha^2}{6\beta} - \frac{\beta}{6} \right) k_{6S}, \end{aligned} \tag{53e}$$

$-\alpha$	$-\beta$	k_{6S}	k_{4S}	$-c_{4K}$
4	3	$1/6$	$1/3$	$1/3$
$9/2$	3	$1/4$	$3/4$	1
4	2	1	2	2.5
$6/5$	2	$1/4$	$8/25$	0.205

(a)

$-\alpha$	$-\beta$	$-k_{6S}$	k_{4S}	c_{4K}
3	2	$1/4$	$1/2$	0
6	4	$1/2$	1	0
3	2	$1/3$	$1/2$	$1/8$
$1/2$	1	$1/4$	$9/4$	5

(b)

TABLE 3: *Solutions to Eq. (54) for $k_{6S} < 0$ and $c_{2K} \geq 0$ (a) or $k_{6S} > 0$ and $c_{2K} < 0$ (b).*

$$
\begin{aligned}
c_{10K} \;=\; & c_{10K}^{(0)} + \frac{(\alpha - \beta)^2 (24\alpha^4 - 24\alpha^3\beta + 12\alpha^2\beta^2 - 4\alpha\beta^3 + \beta^4)}{24\beta^5} \\
& - \left(\frac{3\alpha}{4} + \frac{3\alpha^5}{2\beta^4} - \frac{17\alpha^4}{4\beta^3} + \frac{9\alpha^3}{2\beta^2} - \frac{19\alpha^2}{8\beta} - \frac{\beta}{8} \right) k_{4S} \\
& - \left(\frac{3\alpha}{16} - \frac{\alpha^4}{4\beta^3} + \frac{5\alpha^3}{8\beta^2} - \frac{17\alpha^2}{32\beta} - \frac{\beta}{32} \right) k_{4S}^2 \\
& - \left(\alpha + \frac{\alpha^4}{\beta^3} - \frac{8\alpha^3}{3\beta^2} + \frac{5\alpha^2}{2\beta} + \frac{\beta}{6} \right) k_{6S} \\
& - \left(\frac{3\alpha}{4} + \frac{\alpha^3}{2\beta^2} - \frac{9\alpha^2}{8\beta} - \frac{\beta}{8} \right) k_{8S}.
\end{aligned}
\tag{53f}
$$

From Eqs. (13) and (20) we infer that a resolution to the η problem of FHI requires $V_{\mathrm{HI}}'' = 0$ – needless to say that there is no contribution to η from the term including the c_{1K} coefficient in Eq. (13). Consequently, the η problem of FHI can be alleviated, if we demand:

$$
c_{2K} = 0
\tag{54}
$$

Moreover, the favored by the data on n_{s} hilltop FHI can be attained for $c_{4K} < 0$. Solutions of Eq. (54) satisfying the latter restriction are listed in Table 3-(a). We observe that $k_{6S} > 0$ is beneficial for the latter result, since it decreases c_{4K}, without disturbing the fulfilment of Eq. (54). Another set of solutions can be taken for $\alpha = 0$. In this case – which resembles the cases studied in Ref. [21] –, we get

$$
c_{4K} = 3/4,\ 0,\ -3,\ -6, -9 \quad \text{for } k_{4S} = -\beta = 1 \text{ and } k_{6S} = 0, 1/2, 5/2, 9/2, 13/2.
\tag{55}
$$

On the other hand, $c_{4K} \geq 0$ is still marginally allowed. Solutions to Eq. (54) with the latter resulting c_{4K}'s are arranged in Table 3-(b). In both cases, the extracted k_{4S} are confined in the range $0.1 - 10$, which we consider as being natural. Note that the realization of FHI in nmSUGRA – see Sec. 5.3 – or nnmSUGRA – see Sec. 6.3 – requires a significantly lower $|k_{4S}|$, i.e., $10^{-3} \lesssim |k_{4S}| \lesssim 0.1$.

More generically, taking α, β and k_{6S} as input parameters we can assure the fulfillment of Eq. (54) constraining k_{4S} via Eq. (53b) and find c_{4K} through Eq. (53c). Working this way, we plot in Fig. 9 (left [right] graph) $-c_{4K}$ [k_{4S}] versus $-\alpha$ for $\beta = -2$ and various
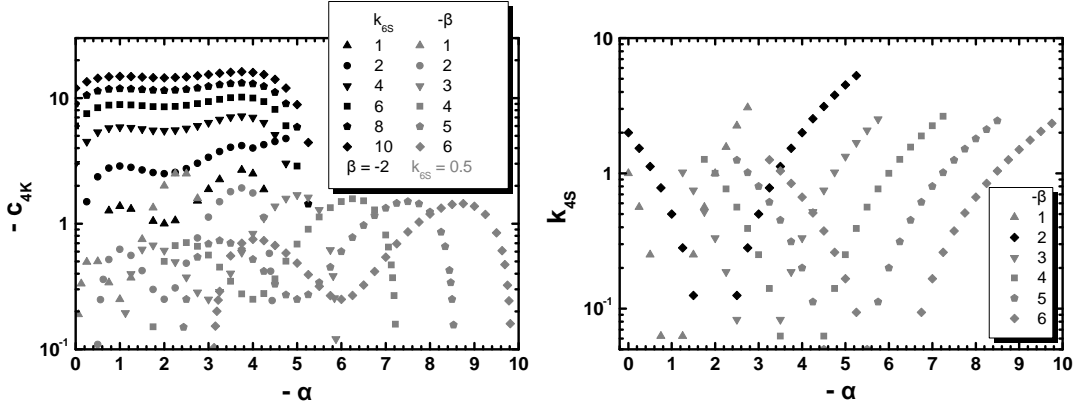
FIGURE 9: *Values of $-c_{4K}$ obtained from Eqs. (53c) and (54) (left plot) and the resulting k_{4S}'s from Eqs. (53b) and (54) (right plot) versus $-\alpha$ for $\beta = -2$ and various k_{6S}'s (black points) or $k_{6S} = 0.5$ and various β's (gray points). The adopted values for the remaining parameters – k_{6S} and β – are also shown.*

k_{6S}'s (black points) or $k_{6S} = 0.5$ and various β's (gray points). The adopted values for all the free parameters employed are also shown. From the right plot of Fig. 9 we remark that the derived k_{4S}'s can be characterized as natural since the majority of them are of order 1. These are independent from the used k_{6S}'s since Eq. (14b) does not contain k_{6S}. From the left plot of Fig. 9, we notice that a wide range of negative c_{4K}'s can be produced which, however, can be bounded from above by the result $|c_{4K}| \leq 16$. As we show in Sec. 7.3, these c_{4K}'s can assist us to achieve hilltop FHI consistently with Eq. (28) for a broad range of κ's or M_S's.

7.2   STRUCTURE OF THE INFLATIONARY POTENTIAL

For σ close to σ_*, V_{HI} given in Eq. (15) can be approximated as

$$V_{\mathrm{HI}} \simeq V_{\mathrm{HI0}} \left(1 + c_{\mathrm{HI}} + c_{4K} \frac{\sigma^4}{4m_{\mathrm{P}}^4} - c_{6K} \frac{\sigma^6}{8m_{\mathrm{P}}^6} \right), \tag{56}$$

where Eq. (54) is taken into account. As in the case of nnmSUGRA, a possible ugly run-away behavior of the resulting V_{HI} can be evaded by the inclusion of higher order terms in the expansion of Eq. (13) – see Eq. (15).

For $c_{4K} < 0$, V_{HI} reaches a maximum at $\sigma = \sigma_{\max}$ which can be estimated as follows:

$$V'_{\mathrm{HI}}(\sigma_{\max}) = 0 \;\; \Rightarrow \;\; \sigma_{\max} \simeq \begin{cases} \left(\kappa^2 \mathsf{N}/8\pi^2 \, |c_{4K}| \right)^{1/4} & \text{for standard FHI}, \\ \left(\kappa^2/4\pi^2 \, |c_{4K}| \right)^{1/4} & \text{for shifted FHI}, \\ \left(8\mu_{\mathrm{S}}^2 M_{\mathrm{S}}^2/27 \, |c_{4K}| \right)^{1/8} & \text{for smooth FHI}, \end{cases} \tag{57}$$

with $V''_{\mathrm{HI}}(\sigma_{\max}) < 0$. Since the behavior of V_{HI} at large σ's is dominated by the higher powers of σ in Eq. (15), as in the case of Sec. 6, V_{HI} can develop a minimum which is located at $\sigma = \sigma_{\min}$ given by Eq. (48).
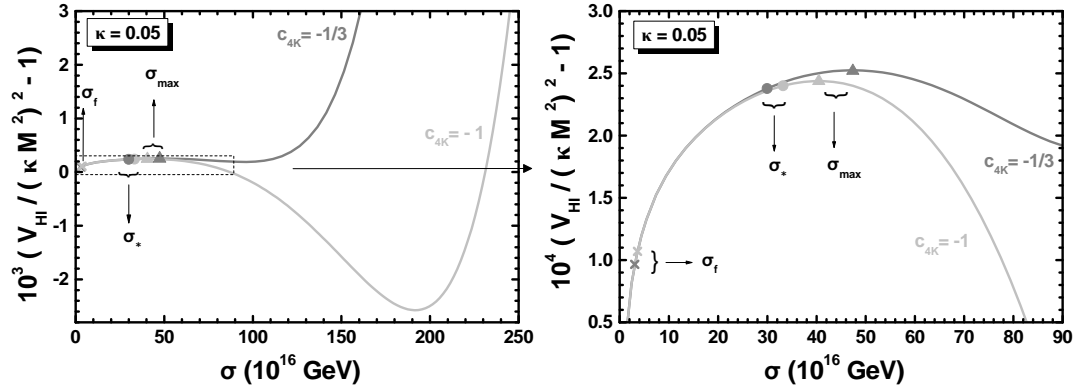
FIGURE 10: *The variation of $V_{\rm HI}$ in Eq. (56) as a function of σ for standard FHI in hSUGRA, $\kappa = 0.05$, $k_{8S} = -3$, $k_{10S} = -k_{12S} = -0.5$ and $c_{4K} = -1/3$ ($n_{\rm s} = 0.969$) [$c_{4K} = -1$ ($n_{\rm s} = 0.945$)](gray [light gray] line). The values of $\sigma_{\rm max}$, σ_* and $\sigma_{\rm f}$ are also depicted.*

This structure of $V_{\rm HI}$ is visualized in Fig. 10 where we display its variation as a function of σ for $\sigma_{\rm c} \leq \sigma \leq m_{\rm P}$ [$\sigma_{\rm c} \leq \sigma \leq 2.5\sigma_*$] (left [right] plot) for standard FHI in hSUGRA, $\kappa = 0.05$, $k_{8S} = -3$, $k_{10S} = -k_{12S} = -0.5$ and $c_{4K} = -1/3$ (gray line) or $c_{4K} = -1$ (light gray line). The parameters α, β, k_{4S} and k_{6S} which lead to the selected c_{4K}'s are shown in Table 3-(a). In the first case (gray line) we obtain $n_{\rm s} = 0.969$ with $\Delta_{\rm m*} = 0.32$ whereas in the second one, we get $n_{\rm s} = 0.945$ with $\Delta_{\rm m*} = 0.17$. This result signalizes the presence of a rather severe tuning needed in order to implement hilltop FHI as anticipated in Sec. 3.3. It is also clear that the minimum-maximum structure of $V_{\rm HI}$ remains in both cases with the second case being much more evident. The values of σ_* and $\sigma_{\rm f}$ are also depicted.

7.3 RESULTS

Our strategy in the numerical investigation of the hSUGRA scenario is the one described in Sec. 4.2. In addition to the parameters manipulated there, we have here the parameter c_{4K} which can be adjusted in order to fulfill Eq. (28) whereas the boundedness of $V_{\rm HI}$ is controlled by the $k_{2\nu S}$'s with $3 \leq \nu \leq 6$. We finally check if the required c_{4K}'s can be derived from Eqs. (53b), (53c) and (54) and the validity of Eq. (31). Our numerical results are presented in Sec. 7.3.1 for standard FHI and in Sec. 7.3.2 for shifted and smooth FHI.

We can, however, do some preliminary estimations for the expected $n_{\rm s}$'s, following the steps described above Eq. (35). In particular we find:

$$n_{\rm s} \simeq \begin{cases} 1 - 1/N_{\rm HI*} + 3\kappa^2 {\sf N} N_{\rm HI*} c_{4K}/4\pi^2 & \text{for standard FHI,} \\ 1 - 1/N_{\rm HI*} + 3\kappa^2 N_{\rm HI*} c_{4K}/2\pi^2 & \text{for shifted FHI,} \\ 1 - 5/3N_{\rm HI*} + 4c_{4K}\left(6\mu_{\rm S}^2 M_{\rm S}^2 N_{\rm HI*}\right)^{1/3} & \text{for smooth FHI.} \end{cases} \tag{58}$$

From the expressions above, we can easily infer that $c_{4K} < 0$ can diminish significantly $n_{\rm s}$. To this end, in the cases of standard and shifted FHI, $|c_{4K}|$ has to be of order unity for
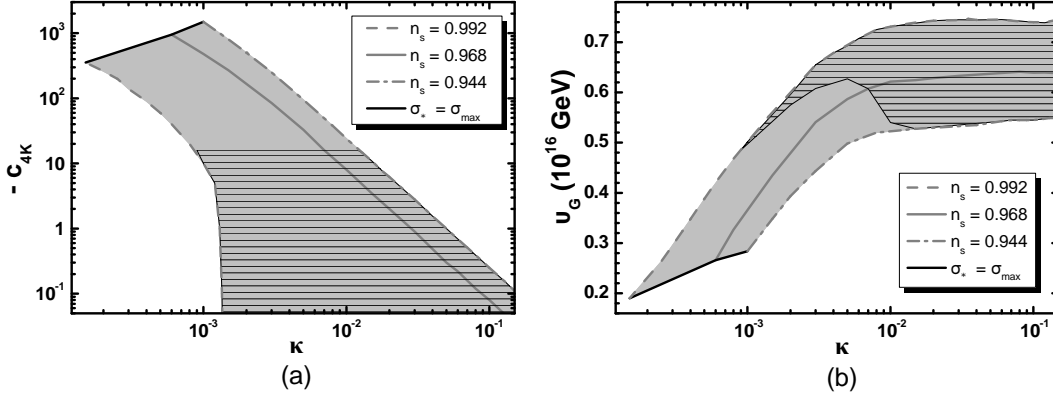
FIGURE 11: *Allowed (lightly gray shaded) regions, as determined by Eqs. (26)-(29), in the $\kappa - c_{4K}$ [$\kappa - v_G$] plane (a) [(b)] for standard FHI in hSUGRA with $c_{2K} = 0$. Ruled is the region which can be covered by the values of α, β and k_{4S} depicted in Fig. 9. The conventions adopted for the various lines are also shown.*

relatively large κ's and much larger for lower κ's whereas, for smooth FHI, a rather low $|c_{4K}|$ is enough.

7.3.1 STANDARD FHI

In Fig. 11-(a) [Fig. 11-(b)] we delineate the (lightly gray shaded) regions allowed by Eqs. (26) – (29), in the $\kappa - c_{4K}$ [$\kappa - v_G$] plane for standard FHI. The conventions adopted for the various lines are also shown in the r.h.s of each graph. In particular, the black solid [dashed] lines correspond to $n_s = 0.992$ [$n_s = 0.944$], whereas the gray solid lines have been obtained by fixing $n_s = 0.968$ – see Eq. (28). Below the black solid line, our initial assumption $\sigma_* < \sigma_{\max}$ is violated. The various lines terminate at $\kappa = 0.15$, since for larger κ's the two restrictions in Eqs. (26) and (27) cannot be simultaneously met. Note that for $n_s = 0.992$ and $1.3 \cdot 10^{-3} \lesssim \kappa \lesssim 0.15$ the curve is obtained for positive $0 \lesssim c_{4K} \lesssim 0.025$, not displayed in Fig. 11-(a).

From our data, we can deduce that (i) v_G, c_{4K} and Δ_{m*} increase with n_s, for fixed κ and (ii) c_{4K} and Δ_{m*} increase with κ, for fixed n_s. Comparing Fig. 11-(a) and Fig. 9-(a), we observe that the required c_{4K}'s, in order to achieve n_s's within the range of Eq. (28), can be derived from the fundamental parameters of the proposed Kähler potentials – see Eqs. (12) and (52) – in a wide range of parameters which is depicted as hatched portions of the light gray areas in Fig. 11. In particular, for $n_s = 0.968$ we obtain

$$0.7 \lesssim \frac{\kappa}{10^{-2}} \lesssim 15, \ \ 6.1 \lesssim \frac{v_G}{10^{15} \text{ GeV}} \lesssim 6.4, \tag{59a}$$

$$16 \gtrsim -c_{4K} \gtrsim 0.035 \ \text{and} \ 0.30 \lesssim \Delta_{m*} \lesssim 0.33. \tag{59b}$$

Note that the v_G's encountered here are lower than those required by Eq. (30). In this case also, as for nmSUGRA and nnmSUGRA – see Secs 5.3.1 and 6.3.1 –, a certain degree of tuning is required as can been seen from the values of Δ_{m*} above.

SHIFTED FHI				SMOOTH FHI			
c_{4K}	-6	-2.5	3	c_{4K}	-0.205	0	$1/8$
$\Delta_{\mathrm{m}*}/10^{-1}$	3.9	5	$-$	$\Delta_{\mathrm{m}*}/10^{-2}$	8.3	$-$	$-$
$\sigma_*/10^{16}$ GeV	3.8	3.7	3.8	$\sigma_*/10^{16}$ GeV	25.6	27	28.1
$\kappa/10^{-3}$	9	9.1	9.3	$M_{\mathrm{S}}/5\cdot10^{17}$ GeV	1.97	1.5	1.3
$M/10^{16}$ GeV	2.28	2.29	2.3	$\mu_{\mathrm{S}}/10^{16}$ GeV	0.083	0.11	0.13
$1/\xi$	4.32	4.35	4.4	$\sigma_{\mathrm{f}}/10^{16}$ GeV	13.4	13.4	13.4
$N_{\mathrm{HI}*}$	52.2	52.2	52.3	$N_{\mathrm{HI}*}$	52.4	52.6	52.7
n_{s}	0.973	0.978	0.986	n_{s}	0.946	0.974	0.991
$-\alpha_{\mathrm{s}}/10^{-4}$	1.9	2.6	4.3	$-\alpha_{\mathrm{s}}/10^{-4}$	4.7	6.5	8.1

TABLE 4: *Input and output parameters consistent with Eqs. (26)-(30) for shifted (with $M_{\mathrm{S}} = 5\cdot10^{17}$ GeV) or smooth FHI in hSUGRA and selected c_{4K}'s indicated in Table 3. To ensure the boundedness of V_{HI} in the case of shifted [smooth] FHI we take $k_{8S} = -15, k_{10S} = -8$ and $k_{12S} = -0.5$ [$k_{8S} = -1$ and $k_{10S} = -k_{12S} = -0.5$].*

7.3.2 SHIFTED AND SMOOTH FHI

In the cases of shifted and smooth FHI, the achievement of Eq. (30) is possible and so, we can confine ourselves to solutions consistent with Eqs. (26) – (30) in Table 4. The selected c_{4K}'s here can be generated by the initial parameters $(\alpha, \beta, k_{4S}$ and $k_{6S})$ of our model as shown in Table 3-(a) and Eq. (55) for $c_{4K} < 0$ and Table 3-(b) for $c_{4K} \geq 0$. The entries without a value assigned for $\Delta_{\mathrm{m}*}$ refer to cases in which V_{HI} has no distinguishable maximum. From the data collected in Table 4 we observe the following:

- In the case of shifted FHI, the required κ's for fulfilling Eq. (30) come out to be rather low and so, the reduction of n_{s} to the level dictated by Eq. (28) requires rather high c_{4K}'s which in turn ask for large k_{6S}'s too. As a consequence, the boundedness of V_{HI} is affected since $-c_{6K}$ in Eq. (15) becomes negative and rather large k_{8S}'s, k_{10S}'s and k_{12S}'s (we here pose $k_{8S} = -15, k_{10S} = -8$ and $k_{12S} = -0.5$). The lowest possible n_{s} achieved with bounded V_{HI} from below is 0.973 which lies within the 68% c.l. observationally allowed margin – see Eq. (28).

- In the case of smooth FHI, n_{s} turns out to be quite close to its central value in Eq. (28) even with $c_{4K} = 0$. Therefore, in order to reach the central and the lowest value of n_{s} in Eq. (28), one needs rather small c_{4K}'s, which may be obtained from our initial parameters – see Fig. 9-(a). However, the resulting $\Delta_{\mathrm{m}*}$'s are lower than those of shifted FHI. On the other hand, the boundedness of V_{HI} is not disturbed here and can be assured for natural values of k_{8S}, k_{10S} and k_{12S} (we use $k_{8S} = -1$ and $k_{10S} = -k_{12S} = -0.5$).

8 CONCLUSIONS

We reviewed the basic types (standard, shifted and smooth) of FHI employing four possible embeddings in SUGRA. Each of these can be characterized by the adopted Kähler potential. In our work, we considered a quite generic Kähler potential in Eq. (12), from which the various SUGRA scenaria can be deduced. In particular, the Kähler potential of mSUGRA, nmSUGRA and nnmSUGRA can be determined by Eq. (12) substituting Eqs. (33), (38a) and (45a) respectively, whereas the one of hSUGRA can be derived by Eqs. (12) and (52). A crucial difference between hSUGRA and the other scenaria is that in hSUGRA we have taken into account contributions to inflationary potential, $V_{\rm HI}$ in Eq. (15), originating by extra (hidden-sector) fields obeying a string-inspired Kähler potential. The resulting forms of $V_{\rm HI}$ implementing FHI in mSUGRA, nmSUGRA, nnmSUGRA and hSUGRA are written in Eqs. (34), (39), (46) and (56) respectively.

We confronted the considered models of FHI with a number of observational data and theoretical requirements which are (i) the need for a solution to the horizon and flatness problems of the SSB cosmology – Eq. (26) (ii) the constraints on $\Delta_{\mathcal{R}}$, $n_{\rm s}$ and $\alpha_{\rm s}$ as result fitting the WMAP7 data by the ΛCDM model – see Eqs. (27), (28) and (29); (iii) the grand unification of the gauge coupling constants – Eq. (30); (iv) the boundedness, the convergence and the monotonicity of $V_{\rm HI}$ – see Eq. (31). Our findings can be summarized as follows:

- FHI in mSUGRA: The predicted $n_{\rm s}$ is just marginally consistent with the observational data, since Eq. (28) is fulfilled either beyond its 68% c.l. or for rather tuned values of κ close to 10^{-5} due to the presence of the tadpole term in $V_{\rm HI}$ with ${\rm a}_S \sim 1\,{\rm TeV}$. Eq. (30) can be met only for shifted and smooth FHI.

- FHI in nmSUGRA: Acceptable $n_{\rm s}$'s can be obtained by restricting the parameter $k_{4S} > 0$ involved in $V_{\rm HI}$ to rather low values (of order 10^{-3}). Enforcing the validity of Eq. (31), the reduction of $n_{\rm s}$ below around 0.95 is prevented. The status of Eq. (30) is as in mSUGRA.

- FHI in nnmSUGRA: By constraining the parameters $k_{4S} < 0$ and $k_{6S} > 0$ of $V_{\rm HI}$ to values of order 10^{-2} and 10^{-1} respectively, we can achieve $n_{\rm s}$'s compatible with data. Eq. (30) can be attained in all the models of FHI. We remark a sizable enhancement of $|\alpha_{\rm s}|$ whereas r remains well below its WMAP7 upper bound in [11].

- FHI in hSUGRA: The two extra parameters (α and β) contained in the Kähler potential of the extra fields give us the chance to eliminate the mass-squared term from $V_{\rm HI}$ for natural k_{4S}'s and k_{6S}'s and generate suitable c_{4K}'s aiming at reducing $n_{\rm s}$ to an acceptable level. Eq. (31) can be satisfied only if $c_{4K} \geq 0$ which gives observationally less interesting $n_{\rm s}$'s. Eq. (30) can be met as in mSUGRA.

Given that from the imposed requirements Eqs. (26), (27) and (29), the convergence and the boundedness of $V_{\rm HI}$ are fulfilled by all the considered settings of FHI, we are left with a subset of requirements – hierarchically represented by Eqs. (28), (30) and (31) – which, in

REQUIREMENTS	TYPES OF FHI		
	STANDARD	SHIFTED	SMOOTH
mSUGRA – see Eq. (34)			
Eq. (28)	$\sim$	$\sim$	$\times$
Eq. (30)	$\times$	$\checkmark$	$\checkmark$
Eq. (31)	$\checkmark$	$\checkmark$	$\checkmark$
nmSUGRA – see Eq. (39)			
Eq. (28)	$\checkmark$	$\checkmark$	$\checkmark$
Eq. (30)	$\times$	$\checkmark$	$\checkmark$
Eq. (31)	$\sim$	$\sim$	$\checkmark$
$0.1 \leq |k_{4S}| \leq 10$	$\times$	$\times$	$\times$
nnmSUGRA – see Eq. (46)			
Eq. (28)	$\checkmark$	$\checkmark$	$\checkmark$
Eq. (30)	$\checkmark$	$\checkmark$	$\checkmark$
Eq. (31)	$\sim$	$\times$	$\checkmark$
$0.1 \leq |k_{4S}| \leq 10$	$\times$	$\times$	$\sim$
hSUGRA – see Eq. (56)			
Eq. (28)	$\checkmark$	$\sim$	$\checkmark$
Eq. (30)	$\times$	$\checkmark$	$\checkmark$
Eq. (31)	$\times$	$\times$	$\sim$
$0.1 \leq |k_{4S}| \leq 10$	$\checkmark$	$\checkmark$	$\checkmark$

TABLE 5: *Test performance of the studied models of FHI in SUGRA. The symbol $\checkmark$ [$\times$] denotes that the corresponding requirement is [is not] satisfied, whereas the symbol $\sim$ stands for a partial or less natural fulfilment of the requirement.*

conjunction with the naturalness inequality $0.1 \leq |k_{4S}| \leq 10$, can be employed in order to rate the analyzed models. Note that the latter criterion does not apply in mSUGRA where $k_{4S} = 0$ by definition. Also, we do not include the naturalness of k_{6S} in our test, since it is more or less assured in both relevant models (nnmSUGRA and hSUGRA) and so, it does not influence decisively our comparisons. Our four-point test is displayed schematically in Table 5. We respectively use the symbol $\checkmark$, $\times$ or $\sim$ when the corresponding requirement is satisfied, is not satisfied or is partially and/or less naturally satisfied. From our final score, we can infer that no model can be regarded as totally satisfactory, since at least one shortcoming is encountered in all cases. However, smooth FHI in nnmSUGRA or hSUGRA can be qualified as the most promising model – no $\times$ is signed. On the other hand, the most compelling implementation of standard [shifted] FHI is within nnmSUGRA [nmSUGRA] since just one $\times$ is listed. In our last statement we take into account that the four criteria are imposed hierarchically – e.g., the attainment of Eq. (28) is considered as more important than the achievement of Eq. (31).

Throughout our investigation we concentrated on the predictions derived from the re-

alizations of FHI, assuming that we had suitable initial conditions for FHI to take place. For this reason, we paid special attention to the monotonicity of $V_{\rm HI}$, which is crucial for a relatively natural attainment of FHI. In general, it is not clear [22, 23] how the inflaton can reach the maximum of $V_{\rm HI}$ in the context of hilltop inflation. Probably an era of eternal inflation prior to FHI could be useful [28] in order the proper initial conditions to be set.

Let us finally note that a complete inflationary scenario should specify the transition to the radiation dominated era and also explain the origin of the observed baryon asymmetry. For FHI in mSUGRA or nmSUGRA this has been extensively studied – see, e.g., Ref. [6, 7, 10]. Obviously our models preserve many of these successful features of this post-inflationary evolution which may further constrain their parameter space and help us to distinguish the most compelling version of FHI. Moreover, the proposed scenaria will be even more challenged by the measurements of the Planck satellite [38] which is expected to give results on $n_{\rm s}$ with an accuracy $\Delta n_{\rm s} \simeq 0.01$ by the next spring.

REFERENCES

[1] A.H. Guth, *Phys. Rev. D* **23**, 347 (1981);
A.H. Guth and D.I. Kaiser, *Science* **307**,884 (2005) [`astro-ph/0502328`].

[2] D.H. Lyth and A. Riotto, *Phys. Rept.* **314**, 1 (1999) [`hep-ph/9807278`];
A. Mazumdar and J. Rocher, *Phys. Rept.* **497**, 85 (2011) [`arXiv:1001.0993`].

[3] G. Lazarides, *Lect. Notes Phys.* **592**, 351 (2002) [`hep-ph/0111328`];
G. Lazarides, *J. Phys. Conf. Ser.* **53**, 528 (2006) [`hep-ph/0607032`].

[4] E.J. Copeland *et al.*, *Phys. Rev. D* **49**, 6410 (1994) [`astro-ph/9401011`].

[5] G.R. Dvali, Q. Shafi and R.K. Schaefer, *Phys. Rev. Lett.* **73**, 1886 (1994) [`hep-ph/9406319`].

[6] R. Jeannerot *et al.*, *J. High Energy Phys.* **10**, 012 (2000) [`hep-ph/0002151`];
R. Jeannerot, S. Khalil and G. Lazarides, *J. High Energy Phys.* **07**, 069 (2002) [`hep- ph/0207244`];
S. Khalil *et al.*, *Phys. Rev. D* **83**, 063522 (2011) [`arXiv:1010.3657`];
M. Civiletti *et al.*, *Phys. Rev. D* **84**, 103505 (2011) [`arXiv:1104.4143`].

[7] G. Lazarides and C. Panagiotakopoulos, *Phys. Rev. D* **52**, 559 (1995) [`hep-ph/9506325`];
G. Lazarides *et al.*, *Phys. Rev. D* **54**, 1369 (1996) [`hep-ph/9606297`];
R. Jeannerot, S. Khalil, and G. Lazarides, *Phys. Lett. B* **506**, 344 (2001) [`hep-ph/0103229`];
M.U. Rehman and Q. Shafi, *Phys. Rev. D* **86**, 027301 (2012) [`arXiv:1202.0011`];
S. Khalil, Q. Shafi and A. Sil, `arXiv:1208.0731`.

[8] G.R. Dvali, G. Lazarides and Q. Shafi, *Phys. Lett. B* **424**, 259 (1998) [`hep-ph/9710314`].

[9] G. Lazarides and Q. Shafi, *Phys. Rev. D* **58**, 071702 (1998) [`hep-ph/9803397`].

[10] G. Lazarides and Q. Shafi, *Phys. Lett. B* **258**, 305 (1991);
K. Kumekawa, T. Moroi and T. Yanagida, *Prog. Theor. Phys.* **92**, 437 (1994) [hep-ph/9405337];
G. Lazarides, R.K. Schaefer and Q. Shafi, *Phys. Rev. D* **56**, 1324 (1997) [hep-ph/9608256].

[11] E. Komatsu *et al.* [WMAP Collaboration], *Astrophys. J. Suppl.* **192**, 18 (2011) [arXiv:1001.4538];
http://lamb da.gsfc.nasa.gov/product/map/dr2/parameters.cfm.

[12] E.D. Stewart, *Phys. Rev. D* **51**, 6847 (1995) [hep-ph/9405389];
M. Bastero-Gil and S.F. King, *Nucl. Phys.* **B549**, 391 (1999) [hep-ph/9806477];
G. German, G.G. Ross and S. Sarkar, *Phys. Lett. B* **469**, 46 (1999) [hep-ph/9908380].

[13] A.D. Linde and A. Riotto *Phys. Rev. D* **56**, 1841 (1997) [hep-ph/9703209];
V.N. Şenoğuz and Q. Shafi, *Phys. Lett. B* **567**, 79 (2003) [hep-ph/0305089].

[14] V.N. Şenoğuz and Q. Shafi, *Phys. Rev. D* **71**, 043514 (2005) [hep-ph/0412102];
M.U. Rehman, Q. Shafi and J.R. Wickman, *Phys. Lett. B* **683**, 191 (2010) [arXiv:0908.3896];
K. Nakayama *et al.*, *J. Cosmol. Astropart. Phys.* **12**, 010 (2010) [arXiv:1007.5152].

[15] R.A. Battye *et al.*, *J. Cosmol. Astropart. Phys.* **09**, 007 (2006) [astro-ph/0607339];
G. Lazarides, I.N.R. Peddie, and A. Vamvasakis, *ibid.* **78**, 043518 (2008) [arXiv:0804.3661];
R. Battye, B. Garbrecht and A. Moss, *Phys. Rev. D* **81**, 123512 (2010) [arXiv:1001.0769].

[16] G. Lazarides and C. Pallis, *Phys. Lett. B* **651**, 216 (2007) [hep-ph/0702260];
G. Lazarides and A. Vamvasakis, *ibid.* **76**, 123514 (2007) [arXiv:0709.3362];
G. Lazarides, *Int. J. Mod. Phys. A* **22**, 5747 (2007) [arXiv:0706.1436];
C. Pallis, *AIP Conf. Proc.* **1122**, 368 (2009) [arXiv:0812.0249].

[17] G. Lazarides and C. Pallis, *Phys. Rev. D* **82**, 063535 (2010) [arXiv:1007.1558];
C. Pallis, *PoS CORFU* **2011**, 028 (2011) [arXiv:1207.6351].

[18] K. Dimopoulos *et al.*, *J. Cosmol. Astropart. Phys.* **02**, 018 (2012) [arXiv:1111.1929];
G. Lazarides, *AIP Conf. Proc.* **1467**, 166 (2012) [arXiv:1205.4830].

[19] C. Panagiotakopoulos, *Phys. Lett. B* **402**, 257 (1997) [hep-ph/9703443];

[20] H.P. Nilles, *Phys. Rept.* **110**, 1 (1984);
S.P. Martin, *" Perspectives on supersymmetry II"*, edited by G.L. Kane, p. 1-153 [hep-ph/9709356].

[21] C. Panagiotakopoulos, *Phys. Lett. B* **459**, 473 (1999) [hep-ph/9904284];
C. Panagiotakopoulos, *Phys. Rev. D* **71**, 063516 (2005) [hep-ph/0411143].

[22] M. Bastero-Gil, S.F. King, and Q. Shafi, *Phys. Lett. B* **651**, 345 (2007) [hep-ph/0604198];
B. Garbrecht *et al.*, *J. High Energy Phys.* **12**, 038 (2006) [hep-ph/0605264].

[23] M.U. Rehman, V.N. Şenoğuz, and Q. Shafi, *Phys. Rev. D* **75**, 043522 (2007) [hep-ph/0612023];
G. Lazarides and A. Vamvasakis, *Phys. Rev. D* **76**, 083507 (2007) [arXiv:0705.3786].

[24] C. Pallis, *"High Energy Physics Research Advances"*, edited by T.P. Harrison and R.N. Gonzales (Nova Science Publishers Inc., New York, 2008) [arXiv:0710.3074].

[25] Q. Shafi and J.R. Wickman, *Phys. Lett. B* **696**, 438 (2011) [arXiv:1009.5340];
M.U. Rehman, Q. Shafi and J.R. Wickman, *Phys. Rev. D* **83**, 067304 (2011) [arXiv:1012.0309].

[26] R. Armillis, G. Lazarides and C. Pallis, *work in preparation*.

[27] C. Pallis, *J. Cosmol. Astropart. Phys.* **04**, 024 (2009) [arXiv:0902.0334].

[28] L. Boubekeur and D. Lyth, *J. Cosmol. Astropart. Phys.* **07**, 010 (2005) [hep-ph/0502047];
      K. Kohri, C.M. Lin and D.H. Lyth, *J. Cosmol. Astropart. Phys.* **12**, 004 (2007) [arXiv:0707.3826];
      C.M. Lin and K. Cheung, *J. Cosmol. Astropart. Phys.* **03**, 012 (2009) [arXiv:0812.2731].

[29] W. Buchmuller, L. Covi and D. Delepine, *Phys. Lett. B* **491**, 183 (2000) [hep-ph/0006168].

[30] S.C. Davis and M. Postma, *J. Cosmol. Astropart. Phys.* **04**, 022 (2008) [arXiv:0801.2116];
      S. Antusch *et al.*, *J. Cosmol. Astropart. Phys.* **01**, 040 (2009) [arXiv:0808.2425].

[31] J. Rocher and M. Sakellariadou, *J. Cosmol. Astropart. Phys.* **03**, 004 (2005) [hep-ph/0406120];
      R. Jeannerot and M. Postma, *J. High Energy Phys.* **05**, 071 (2005) [hep-ph/0503146].

[32] T.W.B. Kibble, *J. Phys. A* **9**, 387 (1976).

[33] G. Ballesteros *et al.*, *J. Cosmol. Astropart. Phys.* **03**, 001 (2006) [hep-ph/0601134].

[34] M.Yu. Khlopov and A.D. Linde, Phys. Lett. B **138**, 265 (1984);
      J. Ellis, J.E. Kim, and D.V. Nanopoulos, *ibid.* **145**, 181 (1984).

[35] See e.g. L.E. Ibanez and D. Lust, *Nucl. Phys.* **B382**, 305 (1992) [hep-th/9202046];
      D. Lust, S. Reffert and S. Stieberger, *Nucl. Phys.* **B727**, 264 (2005) [hep-th/0410074].

[36] K. Enqvist, L. Mether and S. Nurmi, *J. Cosmol. Astropart. Phys.* **014**, 11 (2007) [arXiv:0706.2355];
      S. Nurmi, *J. Cosmol. Astropart. Phys.* **01**, 016 (2008) [arXiv:0710.1613].

[37] R. Allahverdi *et al.*, *Phys. Rev. Lett.* **97**, 191304 (2006) [hep-ph/0605035];
      J.C. Bueno-Sanchez *et al.*, *J. Cosmol. Astropart. Phys.* **01**, 015 (2007) [hep-ph/0608299].

[38] Planck collaboration, http://www.rssd.esa.int/index.php?project=Planck.